(12)

POR-2001(EX)
(WT-2001)(EX)
EXTRACTED VERSION

OPERATION DOMINIC, SHOT SWORD FISH

AD-A995 301

Project Officers Report—Project 1.2

Surface Phenomena

G. A. Young, Project Officer
D. E. Phillips
Naval Ordnance Laboratory
Silver Spring, MD

14 August 1964

NOTICE:
This is an extract of POR-2001 (WT-2001), Operation DOMINIC, Shot Sword Fish,
Project Officers Report, Project 1.2.

Extracted version prepared for
 Director
 DEFENSE NUCLEAR AGENCY
 Washington, DC 20305-1000

DTIC
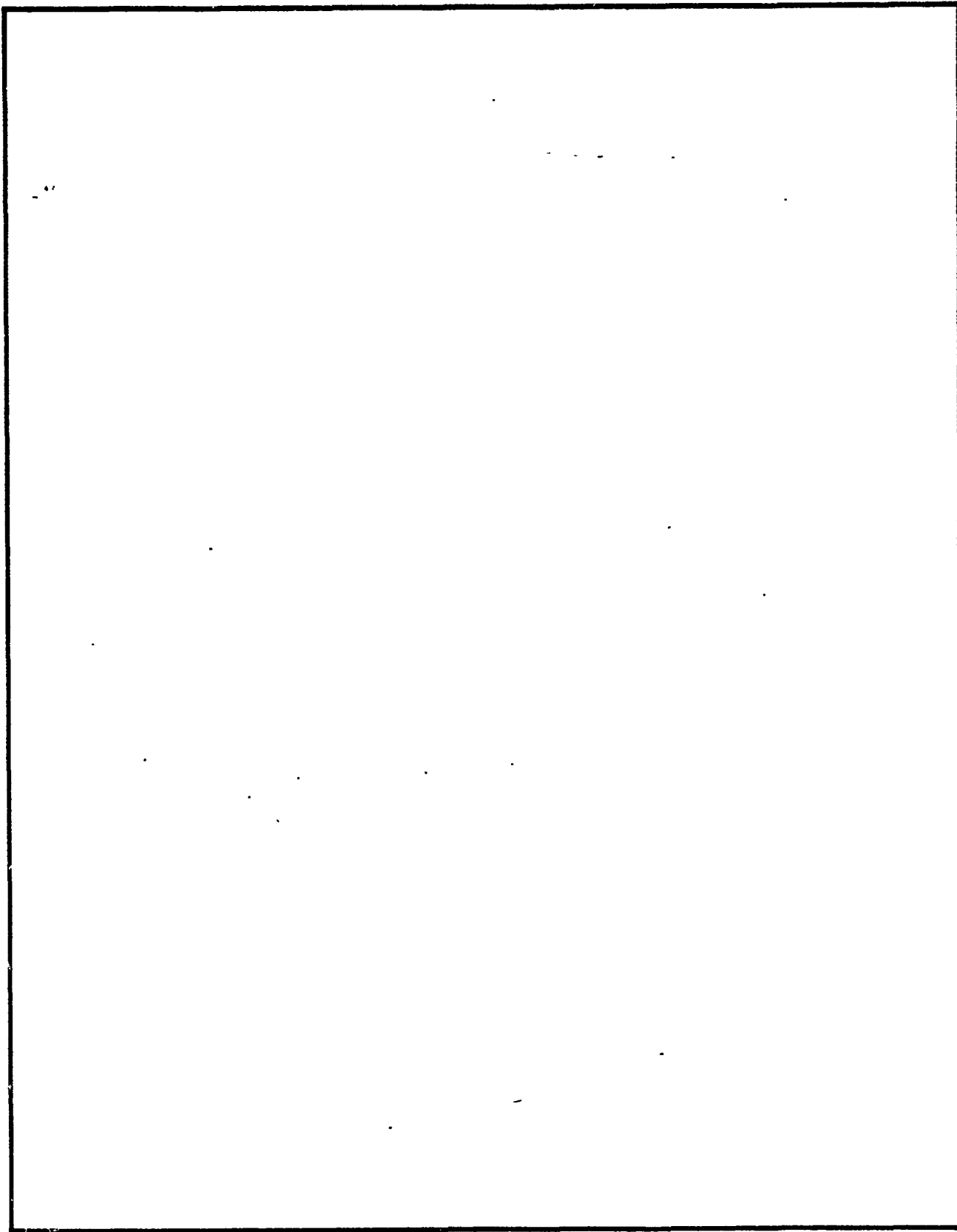ELECTE
DEC 4 1985
B

1 April 1985

DTIC FILE COPY

85 12 2 062

AD-A995301

REPORT DOCUMENTATION PAGE

Form Approved
OMB No. 0704-0188
Exp. Date. Jun 30, 1986

1a REPORT SECURITY CLASSIFICATION UNCLASSIFIED	1b RESTRICTIVE MARKINGS
2a. SECURITY CLASSIFICATION AUTHORITY N/A since Unclassified	3. DISTRIBUTION/AVAILABILITY OF REPORT Approved for public release; distribution is unlimited.
2b. DECLASSIFICATION/DOWNGRADING SCHEDULE N/A since Unclassified	

4 PERFORMING ORGANIZATION REPORT NUMBER(S)	5. MONITORING ORGANIZATION REPORT NUMBER(S) POR-2001(EX) (WT-2001(EX))

6a NAME OF PERFORMING ORGANIZATION Naval Ordnance Laboratory	6b. OFFICE SYMBOL (If applicable)	7a NAME OF MONITORING ORGANIZATION Defense Atomic Support Agency

6c. ADDRESS (City, State, and ZIP Code) Silver Spring, MD	7b ADDRESS (City, State, and ZIP Code) Washington, DC

8a. NAME OF FUNDING/SPONSORING ORGANIZATION	8b. OFFICE SYMBOL (If applicable)	9. PROCUREMENT INSTRUMENT IDENTIFICATION NUMBER

8c. ADDRESS (City, State, and ZIP Code)	10 SOURCE OF FUNDING NUMBERS			
	PROGRAM ELEMENT NO	PROJECT NO	TASK NO	WORK UNIT ACCESSION NO.

11 TITLE (Include Security Classification)
OPERATION DOMINIC, SHOT SWORD FISH, Project Officers Report—Project 1.2 Surface Phenomena, Extracted Version

12. PERSONAL AUTHOR(S)
Young, G.A. and Phillips, D.E.

13a TYPE OF REPORT Project Officers	13b. TIME COVERED FROM _____ TO _____	14 DATE OF REPORT (Year, Month, Day) 640814	15. PAGE COUNT 135

16 SUPPLEMENTARY NOTATION This report has had sensitive military information removed in order to provide an unclassified version for unlimited distribution. The work was performed by the Defense Nuclear Agency in support of the DoD Nuclear Test Personnel Review Program.

17	COSATI CODES		18 SUBJECT TERMS (Continue on reverse if necessary and identify by block number)
FIELD	GROUP	SUB-GROUP	Dominic Photography Plumes
18	3		Sword Fish Underwater Bursts Base Surge
19	4		ASROC Underwater Shock Waves

19. ABSTRACT (Continue on reverse if necessary and identify by block number)

Shot Sword Fish was an operational test of the ASROC antisubmarine weapon system. The general objectives of the project were (1) to record and measure the formation, growth, and dissipation of the visible surface phenomena, including slicks, spray domes, plumes, fallout, base surge, and foam patch resulting from the underwater detonation of an ASROC weapon; (2) to utilize the data obtained to estimate the actual depth of burst, position of burst, yield, and bubble period; (3) to determine the location of ships and platforms in the experimental array before, during and after the test; (4) to provide surface-phenomena time-of-arrival data at platforms and ships in the array for utilization by other projects; and (5) to make the results available for improving the surface-phenomena scaling and prediction techniques which are currently employed for establishing delivery and lethal ranges for fleet nuclear weapons.

In general, there was good agreement between the observed dimensions of the Sword Fish phenomena and the predictions.

20 DISTRIBUTION/AVAILABILITY OF ABSTRACT ☒ UNCLASSIFIED/UNLIMITED ☐ SAME AS RPT ☐ DTIC USERS	21 ABSTRACT SECURITY CLASSIFICATION UNCLASSIFIED
22a NAME OF RESPONSIBLE INDIVIDUAL Betty L. Fox	22b TELEPHONE (Include Area Code) (202) 325-7042 22c OFFICE SYMBOL DNA/STTI

DD FORM 1473, 84 MAR   83 APR edition may be used until exhausted
All other editions are obsolete

FOREWORD

Classified material has been removed in order to make the information available on an unclassified, open publication basis, to any interested parties. The effort to declassify this report has been accomplished specifically to support the Department of Defense Nuclear Test Personnel Review (NTPR) Program. The objective is to facilitate studies of the low levels of radiation received by some individuals during the atmospheric nuclear test program by making as much information as possible available to all interested parties.

The material which has been deleted is either currently classified as Restricted Data or Formerly Restricted Data under the provisions of the Atomic Energy Act of 1954 (as amended), or is National Security Information, or has been determined to be critical military information which could reveal system or equipment vulnerabilities and is, therefore, not appropriate for open publication.

The Defense Nuclear Agency (DNA) believes that though all classified material has been deleted, the report accurately portrays the contents of the original. DNA also believes that the deleted material is of little or no significance to studies into the amounts, or types, of radiation received by any individuals during the atmospheric nuclear test program.

Accession For

A-1

UNANNOUNCED

ABSTRACT

The formation, growth, and dissipation of the visible surface phenomena caused by an underwater ASROC explosion were recorded by means of technical photography from three ships and four aircraft. Additional information was obtained concerning flight time, sinking time, and miss distance of the ASROC warhead and on the positions of ships and platforms in the array.

A slick was measured to a radius of 4200 feet, followed by a spray dome and cavitation pulse spray ring which covered a 6000-foot-diameter region with spray. The spray dome reached a maximum height of   . - and, about six seconds after the burst, was penetrated by plumes which reached a maximum height of   - and a maximum collapsed diameter of 4300 feet. A second set of plumes appeared at about 33 seconds and attained a maximum height of   A base surge moved about 6100 feet upwind and continued expanding in the downwind and crosswind directions during the entire period of measurement, about six minutes. Residual patches of the surge were visible for about ten minutes after the burst. A foam patch was measured to a diameter of 11,600 feet and was still visible an hour after the burst.

Surface-phenomena measurements indicated a depth of burst of 680 feet. No accurate yield was obtained, although

5

a yield estimate consistent with the radiochemical yield was
obtained from the bubble period as determined from plume
trajectories.

In general, there was good agreement between the observed
dimensions of the Sword Fish phenomena and the predictions.
An exception was spray-dome height, which was about double
the predicted value.

PREFACE

Shot Sword Fish was an underwater weapon-effects test conducted in the Pacific Ocean off the southwest coast of the United States in May 1962 as part of Operation Dominic. Sword Fish was the first fully operational test of the Navy's antisubmarine rocket (ASROC) weapon system in which a nuclear war reserve weapon was expended. Weapons-effects information of importance to the advancement of surface-ship capability to conduct nuclear antisubmarine warfare was obtained. An overall description of the test efforts and a summary of preliminary results may be found in the Sword Fish Scientific Director's Summary Report (Reference 1), which includes general information such as location and time of burst. A guide to Sword Fish reports is included.

The successful attainment of the objectives of this project was the result of the combined effort of a large number of people who worked to fulfill the essential technical requirements and maintain high standards despite the extremely limited time scale. Unfortunately, it is impossible to recognize individually the many people involved. Such recognition must be limited to those who made outstanding contributions; however, the contributions of those who remain anonymous were significant in the success of the project.

Particular appreciation is due to the personnel of the Aeronautical Photographic Experimental Laboratory at Johnsville, Pa., who assembled most of the photographic equipment, and designed and prepared the modifications, mounts, electrical circuitry, controls, and power supplies needed for use aboard the ships and aircraft. In addition, their careful

7

processing of the films resulted in the acquisition of a set of high-quality records which is superior to that usually obtained in nuclear tests.

Many military groups and individuals significantly aided the success of the project. A large measure of credit is due LCDR George E. Smith, the Technical Photographic and Air Operations Officer of Joint Task Group 8.3, who arranged and coordinated the many complicated phases of the photographic effort. The skill of the flight crews of Heavy Photographic Squadron 62 and the Third Marine Aircraft Wing, who manned the photographic aircraft, resulted in the acquisition of excellent photographic records from these stations. The cooperation of personnel of Light Photographic Squadron 63, including use of their facilities, also is appreciated. The seventeen enlisted photographers who manned the surface cameras rapidly learned the operation of unfamiliar equipment and carefully and conscientiously performed their assigned duties.

Personnel from the Naval Ordnance Laboratory also contributed significantly to the success of the project. John Arena and Francis X. Smith of NOL's Photographic Division did an outstanding job in operating equipment and providing technical supervision of the Navy photographers. The Photographic Division also furnished cameras and associated equipment for use in the field. NOL personnel who assisted in the analysis and data reduction task included R. L. Willey, Marjorie N. Coleman, David Gloeckner, and Carl Dodge.

8

CONTENTS

CHAPTER 1

INTRODUCTION

Shot Sword Fish of Operation Dominic was an operational test of the antisubmarine rocket (ASROC) antisubmarine weapon (ASW) system. The weapon was launched from the USS Agerholm (DD-826). It exploded under water at approximately 1302 PDT on 11 May 1962 at a position about 365 nautical miles west of San Diego, California (Reference 1).

1.1 OBJECTIVES

The general objectives of Sword Fish Project 1.2 (surface phenomena measurements by photography) were the following: (1) to record and measure the formation, growth, and dissipation of the visible surface phenomena, including the slicks, spray domes, plumes, fallout, base surge, and foam patch resulting from the underwater detonation of an ASROC weapon (a glossary of surface-phenomena terms is included as Appendix A); (2) to utilize the data obtained to estimate the actual depth of burst, position of burst, yield, and bubble period; (3) to determine the location of ships and platforms in the experimental array before, during, and after the test; (4) to provide surface-phenomena time-of-arrival data at platforms and ships in the array for utilization by other projects; and (5) to make the results available for improving

13

the surface-phenomena scaling and prediction techniques which are currently employed for establishing delivery and lethal ranges for fleet nuclear weapons.

1.2 BACKGROUND

The term "surface phenomena" includes all of the visible disturbances of the water surface which result from the action of an underwater explosion. Measurements of these phenomena are important because they help delineate the operational ranges for delivery ships and aircraft. Although the plumes and domes are capable of doing physical damage, the radiological hazards within the fallout and base surge are usually of greater interest because of the relatively large distances that can be traversed by these phenomena, particularly when transported by the wind.

Measurements of surface phenomena are also useful for obtaining information concerning the nature of an underwater burst. For example, the depth of burst can be calculated from measurements of the spread of the primary slick along the water surface. The time of origin of a second slick, second spray dome, or primary plumes, may be used to estimate the period of the first oscillation of the explosion bubble. The initial vertical velocity of the spray dome is directly related to the peak pressure in the underwater shock wave and can sometimes be used to calculate peak pressures, yield, or depth of burst.

14

Extensive photographic coverage was obtained of the four underwater nuclear tests conducted previously. These include Test Baker of Operation Crossroads, a 23-kt device fired at a depth of 90 feet in 180 feet of water (Reference 2); Operation Wigwam, a 32-kt device fired at a depth of 2,000 feet in 15,000 feet of water (Reference 3); Shot Wahoo of Operation Hardtack, a fired at a depth of 500 feet in 3,200 feet of water (Reference 4); and Shot Umbrella of Operation Hardtack, fired on the bottom in 150 feet of water with a yield of The existing theories and data concerning the surface phenomena of underwater nuclear explosions are summarized in Reference 5.

1.3 DESCRIPTION OF PHENOMENA OF DEEP BURSTS

The surface phenomena of underwater explosions can be divided into two main categories: (1) those produced by the shock waves emitted at the time of the explosion and at bubble minima; and (2) those produced by the mass-motion of the water that accompanies bubble pulsation and emergence above the surface.

1.3.1 Shock-Wave Effects. The shock wave produced by an underwater explosion propagates outward radially at an extremely high velocity, which decreases rapidly, approaching the speed of sound. For a nuclear burst, the following expression gives the relationship between the peak pressure in the spherical shock wave and distance from the explosion (Reference 6):

15

$$p_m = 4.38 \times 10^6 \left(\frac{Y^{1/3}}{r}\right)^{1.13} \qquad (1.1)$$

Where: p_m = peak overpressure in the shock wave, psi

Y = yield, kt

r = distance from the burst or slant range, feet
(There is some disagreement between the symbols
utilized here and those in previous nuclear test
reports. In this POR, the usage of Reference 5
is followed. Reference 5 will become a chapter
of "Underwater Nuclear Explosions" (DASA-1240)
which will have the standardization of terminology
as one of its objectives.)

Equation 1.1 is valid for peak pressures less than 10,000
psi. When the shock wave reaches the surface of the water, it
is reflected as a tension wave. The intersection of the shock
front and the surface is visible from above as a rapidly
expanding ring of darkened water, called the slick. The
velocity of spread of the slick is a function of charge depth
only, providing that the shock wave has slowed down to sonic
velocity and refraction effects are negligible. For this
condition, the equation for the radial spread is (Reference 7):

$$R^2 = 2 d U t + U^2 t^2 \qquad (1.2)$$

Where: R = distance from surface zero along the water

surface, feet

d = depth of burst, feet

U = shock front propagation velocity, ft/sec

t = time, seconds

The downward-moving tension wave is superimposed on the tail of the positive phase of the shock wave. At some depth the net tension becomes sufficient to rupture the water. The surface layer breaks away, producing a region of cavitated water beneath. This region eventually closes, producing a pressure pulse in the water. This phenomenon, referred to as bulk cavitation, is of considerable interest in regard to damage to ships.

In actuality, the underwater shock wave does not undergo total reflection, but a portion of the energy is transmitted across the air-water interface. The magnitude of the transmitted air shock wave relative to the underwater shock wave may be approximated for deep bursts (see Section 1.3.2) by using acoustic theory (Reference 7):

$$\frac{p_{ma}}{p_{mw}} = \frac{2\rho_a c_a}{\rho_w c_w}$$

(1.3)

Where: p_m = peak overpressure in the shock wave, psi

ρ = ambient density of the medium, slugs/ft^3

c = ambient sound speed in the medium, ft/sec

Subscripts a and w refer to air and water, respectively.

When the shock wave reaches the ocean bottom, it is reflected as a positive wave which travels to the surface and produces a secondary slick. Equation 1.2 may be used to calculate the spread of this slick, providing the bottom depth is substituted for the depth of burst. Complex slick patterns are produced if the bottom is irregular or contains layers of material with different acoustic properties.

Shortly after the primary slick appears, the water above the explosion rises vertically to form a white mound of spray called the spray dome. This rising spray results from the particle velocity imparted to the water surface by the reflection of the shock wave and the subsequent breakup of the surface layer into water jets and drops. Directly above the charge, the initial vertical velocity of the surface should be approximately equal to the sum of the particle velocities in the incident and reflected shock waves, which are directed upward

18

and are assumed to be equal in magnitude. At all other positions, the particle velocities in the shock waves have equal and opposite horizontal components which cancel. The resultant vertical velocity of the surface is, therefore, (Reference 7):

$$V_o = \frac{2 (144) p_m \cos \delta}{\rho_w U} \qquad (1.4)$$

Where: V_o = initial vertical velocity of the surface at

a point, ft/sec

δ = angle with the vertical of the line from the

explosion to the point on the surface

(The factor of 144 is included to convert the

units of p_m, which are in psi, to lb/ft^2.)

The ratios of the initial dome velocities along the surface to the initial velocity at surface zero are independent of the yield and may be utilized to estimate the depth of an explosion by means of the following expression (Reference 8):

$$V_o (R) = V_o (0) \left[1 + \left(\frac{R}{d} \right)^2 \right]^{-1.07} \qquad (1.5)$$

Where: $V_o (R)$ = initial spray velocity at a given dome radius,

R, ft/sec

$V_o (0)$ = initial spray velocity at surface zero,

ft/sec

19

The rise of the spray in the dome can sometimes be represented by a parabolic expression of the following form (Reference 9):

$$h = V_o t - ft^2 \qquad \qquad (1.6)$$

Where: h = height of spray dome, feet

  f = retardation coefficient, ft/sec^2

Consequently, the maximum dome height can be calculated from:

$$h_{max} = \frac{V_o^2}{4f} \qquad \qquad (1.7)$$

The values of f for a deep burst are given approximately by (Reference 4):

$$f = 30e^{-0.5\ R/d} \qquad \qquad (1.8)$$

The equation of motion for a water drop which is given an upward vertical velocity and decelerates because of gravity and atmospheric resistance is (Reference 5):

$$\frac{dv}{dt} = -g - 4.94 \times 10^{-3} d^{-1.84} v^{1.16} \qquad (1.9)$$

Where: v = velocity of water drop, cm/sec

g = acceleration due to gravity, cm/sec^2

d = drop diameter, cm

Solutions of Equation 1.9 in terms of height and time are similar to spray dome height-versus-time curves. A comparison of curves with the same initial velocity provides an estimate of the size of water drops in a spray dome.

The maximum extent of the spray from a nuclear burst may be estimated from the following expression (Reference 4):

$$\delta_{max} = 85.3 - 0.021 \frac{d}{Y^{1/3}} \qquad (1.10)$$

1.3.2 Mass-Motion Effects. If an explosion occurs at a deep position, the gaseous explosion products push the surrounding water radially outward at a high velocity. The interface continues accelerating outward until the bubble pressure is equal to that of the hydrostatic pressure. Because of the inertia of the water, however, the bubble continues expanding until the pressure difference brings it to a stop. At this time the pressure of the gas is much lower than the hydrostatic pressure, and the bubble contracts. It reaches

21

a minimum size, at which an abrupt reversal of motion occurs and a pressure wave is emitted. This pressure wave is referred to as the first bubble pulse and the time at which it occurs is termed the first bubble period.

The collapse or contraction of the bubble to its minimum size is not uniform in all directions because of the difference in hydrostatic pressure on the various parts of the bubble. The bubble motion is greatest at the bottom and least at the top. In fact, the bottom of the bubble may impinge on the top and penetrate the water above the bubble in the form of a jet. At the time of the minimum the bubble has the shape of a torus; however, it expands again into a roughly spherical shape.

During the collapse and re-expansion phase the bubble migrates upward. The bottom shows the greatest upward motion during the collapse, and the top shows the greatest upward motion during the expansion. The total motion occurs during a relatively brief period before and after the time of the bubble minimum. The bubble continues to pulsate and migrate upward until it reaches the water surface, or until its energy is dissipated or transferred to the surrounding water.

The maximum bubble radius is (Reference 10):

$$A_{max} = 1500 \ \frac{Y^{1/3}}{Z^{1/3}} \qquad (1.11)$$

Where: A_{max} = maximum bubble radius, feet

Z = total hydrostatic pressure at depth of

burst, feet of water

The expression for the period of the first pulsation, from
the time of detonation until the minimum size is attained, is
(Reference 10):

$$T_1 = \frac{515 \ Y^{1/3}}{Z^{5/6}} \left[1 - 0.10 \frac{A_{max}}{d} \right] \qquad (1.12)$$

Where: T_1 = first bubble period, seconds

The upward migration of a nuclear bubble from the time of
burst until it re-expands to the second maximum radius may be
estimated by means of the following expression (Reference 10):

$$\Delta Z = 3.5 \ Z \left(\frac{A_{max}}{Z} \right)^{3/2} \left[1 - 0.1 \frac{A_{max} Z}{d^2} \right] \qquad (1.13)$$

The maximum bubble radius, period, and migration during
subsequent pulsations may be calculated by the methods presented
in Reference 10.

The gases within a nuclear bubble consist primarily of steam
produced by the vaporization of the surrounding water. The water

23

is continuously vaporized while the bubble expands and the interface is transferred from one set of particles to another. The surface of the bubble is probably not sharply defined, since the density of the moist steam at the interface should be the same as that of the surrounding medium (Reference 10).

A nuclear bubble loses energy not only in oscillation and migration, but also because of the condensation of steam. Its oscillations are therefore rapidly damped. Results from Wigwam and model experiments with steam bubbles indicate that a nuclear bubble will not undergo more than three oscillations (Reference 6).

Although the shock-wave effects at the water surface change gradually if the depth of burst is increased or decreased, the phenomena produced by an explosion bubble as it oscillates and migrates upward may vary drastically with relatively small changes in burst depth. The behavior of the surface is therefore discontinuous in nature and can best be studied by treating each range of depths separately. A complete discussion of these ranges is given in Reference 5; only a brief description of the phenomena for the range within which Sword Fish occurred is presented here.

The Sword Fish burst occurred at a depth of about 680 feet and had a yield of possibly   This depth of burst and yield classify the shot as a deep burst. The shallow limit of this

24

range is defined as the depth at which the bubble becomes tangent to the original water surface at its first maximum expansion. This depth may be determined by setting A_{max} and Z equal to d in Equation 1.11 and is (Reference 5):

$$d = 240 \ Y^{1/..} \tag{1.14}$$

The deep limit of this region is where the bubble ceases to exist in an oscillating form. This occurs after three oscillations and is given by (Reference 10):

$$d = 600 \ Y^{1/4} \tag{1.15}$$

For Sword Fish, $d/Y^{1/4}$ is approximately .

When an explosion bubble collapses to a minimum size, the pressure wave which is generated also may produce a slick and spray dome at the surface. The actual approach of a bubble toward the surface, and its arrival and emergence produce a violent upheaval of the water, which is thrown upward and outward in the form of plumes. A roughly hemispherical mass of plumes is expected to form after a deep burst.

1.3.3 Visible Base Surge. The plumes produced by the emergence of the bubble at the water surface break up into spray as they spread outward. When they collapse, the spray continues to move radially along the water surface as an expanding toroid.

25

This expanding aerosol is called a base surge. Because of the high concentration of spray droplets, air and possibly gaseous explosion products are entrained, and the mixture behaves initially in the same manner as a dense homogeneous fluid.

Following a nuclear burst, a portion of the radioactive fission products enters the base surge. When the water evaporates, the fission products remain as an invisible cloud, or aerosol, which continues to expand. The surge is readily transported by the wind. The wind eventually has a pronounced retarding effect in the upwind direction and the entire surge cloud drifts in the direction of the surface or near-surface winds.

During the early expansion of the surge the main forces governing its flow are inertia and gravity. Froude scaling parameters may therefore be used to reduce the motion for explosions of different magnitudes. In Froude scaling, the time scale factor is equal to the square root of the length scale factor. A more complete discussion of base-surge scaling is given in Reference 5. For the deep-burst category the length scale factor employed is the maximum bubble radius, A_{max}, as given by Equation 1.11. The prototype used for scaling base-surge dimensions in this range is Shot Wahoo of Operation Hardtack. Wahoo surge crosswind radius and time dimensions have

been reduced by the calculated Wahoo maximum bubble radius and its square root, respectively. Thus the crosswind growth of a deep burst may be obtained by multiplying the reduced Wahoo surge dimensions by the calculated maximum bubble radius and its square root. The downwind extent is obtained by adding the wind speed to the crosswind curve. The upwind extent is more difficult to determine; it generally lies between the curves obtained by subtracting one-half the wind speed and the full wind speed from the crosswind curve.

After the primary plumes have collapsed, the oscillation of the disturbed water surface may produce a second upheaval which is large enough to generate secondary plumes. These plumes may form a second surge, smaller than the first, which also spreads outward and later merges with the first.

The continued rise and fall of the surface generates a train of surface waves, which is initially obscured by the base surge. The waves overtake and pass the surge when it slows down.

When the motion of the surface ceases, a roughly circular area of foam remains visible for possibly 30 minutes. The foam patch expands slowly; its edge probably indicates the extent of residual contamination in the water.

CHAPTER 2
PROCEDURE

2.1 GUIDING PRINCIPLES

Because of the expected similarity between Sword Fish and
Shot Wahoo of Operation Hardtack, the Wahoo surface-phenomena
measurements were used in the preliminary preparation for the
technical photographic coverage. Subsequently, these predictions
were refined by using the prediction techniques given in
Reference 4. For planning purposes it was assumed that the wind
speed would be between 5 and 15 knots and that the base surge
would drift with the wind and be visible for up to 20 minutes
after the burst. It was also assumed that the array would be
towed into the wind.

2.2 TECHNICAL PHOTOGRAPHIC COVERAGE

The instrumentation for this project consisted of timed
technical photography. Because of the wide range in size and
rates of growth of the various phenomena, and also because of
the lack of symmetry of many of the phenomena, a relatively
large number of cameras of differing speeds and fields of view
was required. In addition, it was necessary to allow for
uncertainties in yield, depth of burst, and location of the
burst relative to the target.

The photographic plan was devised with the idea of providing at least two cameras as primary sources of data for each of the various phenomena. While other records could be used if these cameras failed, the data obtained would be less accurate.

Initially, three aircraft camera stations and three ship stations were proposed. In the planning stage, one proposed aircraft, in a planned circular flight path at an altitude of 2,000 feet and a horizontal range of 30,000 feet, was eliminated. The remaining stations were considered to be a minimum for successful attainment of the objectives of the project.

The positions of the various camera stations at the time of burst are given in Table 2.1 and are shown graphically in Figure 2.1. Station A-1 consisted of two jet photographic aircraft (A3D-2P) containing duplicate camera equipment, in order to increase the probability of attaining high-speed photography of the early spread of the slick from a position directly above surface zero and also to minimize the time intervals during which aircraft would not be vertically above the towed array. These are referred to as Stations A-1A and A-1B. Camera data for these two stations are given in Tables 2.2 and 2.3. All cameras were aimed vertically downward, except for the T-11 cameras, which were aimed obliquely. The T-11's contained clocks and were used primarily for timing purposes.

29

At the time of burst, these aircraft were flying at an altitude of 20,000 feet and at a heading of 330 degrees True with a drift of 15 degrees to the right. Their speed was about 200 knots, and they were separated by a distance of 2,100 feet. Station A-1A was approximately 3,200 feet beyond surface zero, and Station A-1B was approximately 1,100 feet beyond surface zero.

Each aircraft made additional passes over the towed array. The times, altitudes, and headings for these passes are summarized in Table 2.4. The times of the first three passes for each aircraft were obtained from cameras containing clocks, while the times of the subsequent passes are values recorded by the photonavigator of each aircraft. Headings and altitudes were also recorded by the photonavigators, but in most cases these values have been verified or corrected by observing the known positions and sizes of objects visible on the photographic records. The A-1B aircraft conducted the pre-test mapping run at an altitude of 7,000 feet and the A-1A aircraft conducted the post-test mapping run at an altitude of 10,000 feet.

Station A-2 consisted of two R5D (Douglas DC-4) aircraft to provide adequate space for the mounting of the seven cameras required at this position. These are referred to as Stations A-2C and A-2D. The aircraft were expected to maintain a speed of about 120 knots, circle the array at an altitude of 10,000 feet and a horizontal range of 30,000 feet, and maintain a

30

separation angle of about 45 degrees. Power for the cameras was provided by eight 24-volt wet-cell batteries in a series-parallel arrangement with a maximum output of 96 volts. The cameras in the A-2C aircraft were on a single mount so they could be operated by a single photographer. The cameras in the A-2D aircraft, however, were aimed separately. Camera data for these stations are given in Table 2.5.

The final positions of the surface camera stations were established to a large extent by safety considerations and the locations of ships placed for other purposes. Station S-1 was located on the USS Molala (ATF-106), the fleet tug which towed the array. At the time of burst, this ship was located 19,100 feet from the burst at a bearing of 338 degrees True.

Station S-2 was located on the forecastle of the USS Hopewell (DD-681). The primary purpose of this ship was to track submarine simulators by means of sonar for Project 1.3. It was headed almost directly at surface zero at the time of burst and subsequently maneuvered to evade the base surge and also to recover the simulators. A position-vs-time plot of the Hopewell is shown in Figure 2.2. At the time of burst, the Hopewell was 12,300 feet from surface zero at a true bearing of 19.5 degrees. In addition, this ship tracked the two R5D photo aircraft by means of its fire control radar (see Section 2.7).

Station S-3 was located on the starboard side of the USS Monticello (LSD-35). At the time of burst this ship was 23,600 feet from surface zero at a true bearing of 252 degrees.

With the exception of Station S-2, the motion of the ships relative to surface zero is believed small and is neglected in the measurements. Camera data for the ship camera stations are given in Tables 2.6 through 2.8. All cameras were battery powered, using the same system employed in the R5D's, because of the possibility of power failure aboard ship if the circuit breakers were knocked out by the shock waves.

Personnel at the Naval Ordnance Laboratory (NOL) were responsible for establishing the technical photographic requirements. This included planning the technical photography, incorporating the requirements of other projects into the coverage, and assuring that the necessary photographic requirements were being met when changes were made in the overall operational plan. The acquisition of cameras and photographic aircraft, and the assignment of technical personnel other than those from NOL, were arranged by Joint Task Group (JTG) 8.3. Aircraft operations and the coordination of all technical photographic activities were also the responsibility of JTG 8.3. The Aeronautical Photographic Experimental Laboratory (APEL) of the U. S. Naval Air Development Center, Johnsville, Pennsylvania, was responsible for the preparation of the photographic stations.

This included the overhaul and calibration of over 50 cameras from various Naval establishments, the procurement of film, the mounting of cameras in the aircraft, the design and installation of timing systems in many of the cameras, and the design and fabrication of control and power circuitry for all stations. This was accomplished in a period of approximately two months. In addition, APEL furnished six people for the field phase of Sword Fish and, after the shot, developed and made positive projection prints of all the black-and-white motion-picture film.

All cameras aboard the ships were manually aimed. Seventeen Navy photographers from various units were made available for this purpose. Two photographers from NOL also participated in the test, and personnel from Projects 1.1 and 1.2 assisted in operating the cameras. The two A3D photographic aircraft were from Detachment 35, Heavy Photo Squadron Sixty-Two (VFP-62), Jacksonville, Florida. The R5D aircraft were from Marine Aircraft Repair Squadron 37, Third Marine Aircraft Wing, El Toro, California. The aircraft operated out of the Naval Air Station, Miramar, San Diego, California.

2.3 SUPPORT REQUIREMENTS

Supporting environmental data were requested to properly evaluate the information obtained by photography. These included the following meteorological data: (1) temperature,

33

relative humidity, barometric pressure, wind speed, and wind direction from the surface to an altitude of at least 5,000 feet; and (2) visual observations of cloud cover and measured cloud heights. The following oceanographic data were also requested: (1) water temperature and salinity to the depth of burst; (2) depth of the bottom; and (3) bottom contours in the vicinity of the test. The pertinent information available is summarized in Appendix B. Additional information is also given in Reference 1.

Radar tracking of the ships and aircraft with radarscope or radar panel photography was also requested in order to obtain a permanent record of the locations of the camera stations and other elements of the array.

2.4 SPECIAL PHOTOGRAPHIC PROCEDURES

Unique problems were encountered in the development of the photographic procedures. These arose because of such factors as the unknown location of surface zero, the uncertain time of burst, the constant motion of all cameras, and the possibility of an accidental air burst.

No long-focal-length lenses were used, except for mapping purposes, because the cameras were not fixed and surface zero was not known beforehand with precision. Because of the need for photographs from directly above surface zero when the burst occurred, the countdown was taken over at H-30 seconds by the

34

photonavigator of the lead A3D, who established the missile launch time on the basis of the aircraft's position and speed. The countdown was held at this time for approximately one and one-half minutes to allow the aircraft to attain the proper position. The countdown was then resumed. Cameras were started at launch time, except for the high-speed Millikens and Fastax, which started 30 seconds after the launch occurred. The burst was expected to occur approximately 40 seconds after the missile was launched.

Because of the possibility of an accidental air burst, safety procedures were established to protect the photographers' eyes from retinal burns. It was decided that all photographic personnel would either wear high-density goggles, cover their eyes, or use an Infrared Viewing Set (AN/SAR-4A) during the period from H-10 seconds until it was certain the warhead entered the water. The observation of the splash was to be made with a closed-circuit remotely-operated television camera on the firing ship and was to be announced as part of the countdown.

Photographers trained their cameras at the target prior to H-10 seconds, took protective action until after the splash (a period of about 40 seconds), and then re-aimed the cameras. As the ships were rolling and possibly yawing, this resulted in some cameras being improperly aimed when the burst occurred.

Pre-test experiments indicated that it was not possible to aim the cameras accurately with high-density goggles or Infrared Viewers. However, the latter were used to observe the launch of the missile. This provided a visual backup in case the countdown was not heard at the camera stations.

As the target raft was small (13 by 13 feet) and of low silhouette, four Mark 28 Mod 0 Target Flares were ignited on the target by radio signal to provide improved visibility for photographers between the launch time and burst time. These flares were visible through the Infrared Viewers as well as to the uncovered eye.

2.5 RESULTS OF PHOTOGRAPHIC EFFORT

Only three cameras failed to produce records, although timing was lost on some others. Immediately after the shot, the aircraft motion-picture film was flown to APEL for carefully controlled processing. The films obtained at the surface stations were retained on the ships until they docked at the Naval Repair Facility in San Diego. These films were then carried to NOL by project personnel and delivered to APEL for processing.

The aerial mapping films, including the 70mm and F-56 records obtained from the photographic aircraft, were processed by personnel of Light Photo Squadron Sixty-Three (VAP-63) at the Naval Air Station (NAS), Miramar, California, immediately after the shot. Preliminary analysis of the mapping films was also conducted at Miramar.

Positive projection prints of the motion-picture films were made at APEL for study and measurement by the same quality-control method used for processing the originals. The entire procedure was planned to minimize the possible loss of records, either in transit or by hasty processing of film, and to prevent scratching of the original negatives by projection machines. As a result, high-quality photographs were obtained.

Measurements of the surface phenomena, including rectification of the oblique photographs obtained in the R5D's, were made by Air Survey Corp., of Arlington, Virginia, under contract to NOL (Contract No. N60921-7068). Additional measurements, including analysis of the mapping films, some surface-phenomena measurements, and some rectifications, were made by project personnel at NOL.

While the overall results of the photographic effort are considered satisfactory, some difficulties were encountered which affected the final results. Among these were the failure to observe surface zero in the fields of view of the high-speed Fastax cameras in the A3D's, due in part to the large miss distance of the missile (the second A3D was almost directly over the target raft at burst time); and the failure to run the motion-picture cameras continuously on the A3D's, thus making it difficult to determine the times when the cameras were photographing the event.

2.6 PHOTOGRAPHIC LOCATION OF ELEMENTS OF THE TOWED ARRAY

One of the objectives of Project 1.2 was to determine the positions of the various elements of the towed array before, during, and after the shot. These positions were determined from the vertical photographs obtained from the two A3D aircraft. Included in this report are the locations of the portion of the array upwind of the target raft at approximately one-half hour prior to the shot and less than one second after the burst. Project 2.1 determined the positions of its downwind coracles at the time of burst (Reference 11). Post-burst positions of various elements of the upwind portion of the array are presented relative to the stern of the USS Bausell, as surface zero was not visible. In addition, information on the positions of the three surface camera stations was obtained from the photographic records and is also presented.

2.6.1 <u>Pre-test Mapping Run</u>. The pre-test photomapping run was conducted at an altitude of 7,000 feet rather than at the planned altitude of 10,000 feet because of cloud conditions. This run was made by the second A3D (Station A-1B) using only one camera (Camera No. A-1B-8), although it had originally been intended to operate all the mapping cameras. The field of view of this camera along the flight path of the aircraft was only 1,750 feet at this altitude; thus, in general, only two or three objects appeared on each frame.

To determine the locations of the elements relative to the target raft, a rectangular coordinate system was set up with the Y axis pointing along the flight path of the aircraft (345 degrees True). The X and Y coordinates of each element were then determined. By adding the components in succession, the coordinates of each element relative to the target were obtained. These were then converted to ranges and bearings relative to the target raft, which are presented in Table 2.9.

The field of view of the camera was not sufficient to include both the target raft and Platform 2 on the same frame. It was therefore necessary to determine this distance from the actual shot run, using the same record.

2.6.2 Locations at Shot Time. The locations of the upwind elements of the towed array at the time of the explosion were determined from two camera records (A-1B-6 and A-1B-8). Only one frame was measured on each record, that being the frame which showed the first visible surface effect. The location of surface zero was determined by locating the center of the circular shock-wave slick. The KA-46 record (A-1B-6) had a sufficiently large field of view and was of such excellent resolution that the entire upwind array from the target raft to Coracle 1 was visible. The CA-13 record (A-1B-8) included the towed array up to Platform 1. No attempt was made to

measure the remaining portion of the array on succeeding frames of this record. Examination of these frames indicated that some motion of the elements close to surface zero (elements which must be used as reference points on the succeeding frames) occurred when the target raft and the towline were lifted upward by the rising spray dome.

In order to compare the relative motion of the tow during the half hour between the photo-mapping run and shot time, values of range and bearing of the various elements relative to the target for both runs are presented in Table 2.9. This possibly does not give an accurate picture because it was necessary to use the distance and bearing from the target raft to Platform 2 from the actual shot run for both sets of data. However, the small differences in the locations of other elements of the array indicate that there was little relative motion during this period. The position of the splash relative to the target is included in this table.

The range and bearing of the elements relative to surface zero at the time of the explosion are probably the most important and useful values for interpreting the data obtained by means of the instrumentation located on these elements. This information is presented graphically in Figure 2.3 and is tabulated in Table 2.10. These values are believed to be accurate to ± 10 feet and to ± 1 degree.

2.6.3 Post-Shot Positions of Towed Array. After the burst, the location of surface zero could not be determined except for the first few minutes. It was therefore necessary to locate the positions of the upwind elements of the array relative to an arbitrary reference point, the stern of the Bausell. Ranges and bearings relative to the Bausell were determined at approximately 10, 16, and 30 minutes after the burst. The positions were obtained from the CA-13 cameras located in the two A3D's and are presented in tabular form in Table 2.11. No positions were determined prior to 10 minutes, as the base surge and foam patch obscured all but the Bausell and the outermost two coracles.

At H + 10 minutes the two platforms and Coracle 3 lay fairly close together within and near the edge of the foam patch. They were approximately 2,000 feet astern of the Bausell at a bearing of about 180 degrees True relative to the stern. They were probably moved to this position by the violent action of the explosion and by the upwelling and vortex-like flow of water about surface zero. At H + 16 minutes these same elements were still fairly close together and were still located within the foam patch. However, their bearing relative to the stern of the Bausell had changed by about 20 degrees, possibly caused by tightening of the towline, as they had swung to a position almost directly astern of the

41

ship. At H + 30 minutes the array was definitely being towed away from the burst point, as the elements had streamed out astern of the Bausell. Coracle 3 was located alongside Platform 1 during the entire period up to 30 minutes after the burst, possibly caused by a tangling of the towline.

While it is impossible to determine the motion of the Bausell, an approximate indication can be obtained by observing the relative motion of the elements, particularly Platforms 1 and 2. At the time of burst, the two platforms were 1160 feet apart. Thirty minutes after the burst they were 875 feet apart, indicating the towline was not yet taut between the two platforms. This was further substantiated on the photographs, which showed that at H + 30 minutes Platform 2 had not yet swung around to the heading it would be expected to have if it were being towed. Between H + 16 and H + 30 minutes, these two platforms had separated a distance of 617 feet. If this is indicative of the speed of the tow, then the Bausell was moving at an average speed of about 0.4 knot. While this estimate is crude, it is in agreement with the preshot concept of the tow ship just keeping steerageway, estimated to be about 1 knot.

2.6.4 Determination of the Locations of the Surface Camera Stations. In addition to determining the locations of the elements in the tow, it was also possible to determine the

positions of the surface camera stations at the time of burst by use of the overhead aerial and/or the surface photographs. The ship positions actually were measured to the mid-point of each ship; however, the difference between these points and the locations of the cameras was negligible. The position of the USS Molala (Station S-1) was determined from aerial photographs. These photographs indicated that this ship was 19,100 feet from surface zero at a bearing of 338 degrees True at the time of burst. Its bearing was also obtained by observing the position of the burst relative to the Bausell as seen from the Molala. The Bausell was at a bearing of 338 degrees True and, as viewed from the Molala, the burst occurred slightly to the left of the Bausell. However, the angle measured between the Bausell and the burst was only 26 minutes.

The position of the USS Hopewell (Station S-2) was obtained from both aerial and surface photographs. The aerial photographs indicated that the Hopewell was 12,300 feet from the burst and at a bearing of 19.5 degrees True. This position was also indicated by observing the known positions of the upwind elements of the tow on photographs obtained on the Hopewell, and by observing the position of the Hopewell relative to the Bausell as seen from the Monticello.

43

The position of the USS Monticello (Station S-3) was determined by observing the known positions of the upwind elements of the tow. The range determined by this method was 23,600 feet, and a bearing of 252 degrees True was obtained.

The ranges and bearings of these ships agreed to within 1 1/2 percent of those obtained by radar and shock wave arrival times, and the bearings agreed to within 2 to 3 degrees. Arrival times and radar positions are reported in Reference 1. The values determined by photographic means have been used in the analysis of the photographic records for this report.

2.7 RADAR TRACKING OF THE R5D PHOTOGRAPHIC AIRCRAFT

Continuous radar tracking of the two R5D aircraft was accomplished with the two fire-control radar systems located on the Hopewell. The Mark 56 fire-control radar tracked the first R5D (Station A-2C) and the Mark 37 fire-control radar tracked the second R5D (Station A-2D). The location of each aircraft was recorded by photographing the range and bearing dials of each radar system. Automax data-recording cameras (modified 35mm Traids), operated by intervalometers at a rate of one frame every two seconds, were used to photograph the dials. A stop watch was also photographed so that the exact frame rate could be established.

44

The Mark 56, which is located in the after part of the ship, tracked its aircraft until about 30 seconds before launch time, when it lost it in the ship's superstructure (the aircraft being directly off the bow). The aircraft was re-acquired about three minutes after the burst and was tracked until about 25 minutes after burst time. The Mark 37 tracked its aircraft until burst time, when the radar was put out of operation by the effects of the underwater shock waves. It resumed tracking the aircraft about 11 minutes later and continued tracking until 25 minutes after the burst.

The Station A-2C aircraft, when it was lost by the radar, was at a horizontal distance of 31,300 feet from surface zero at a true bearing of 196 degrees. Examination of the photographic records indicates that the aircraft was still at the same horizontal range but at a true bearing of about 150 degrees from surface zero at burst time. The position of the A-2D aircraft at the time of burst, as determined from radar information, was at a horizontal range of 35,700 feet and at a true bearing of 230 degrees relative to surface zero. However, photographs indicated its bearing as 250 degrees True. Because of the general lack of success in the radar tracking of the photo aircraft, an alternate method of rectifying the oblique photographs was employed. This method made use of the visible horizon on the photographs to determine the declination angle

45

of the camera, plus visible objects on the water surface to determine the relationship of the photograph to True North. These are the two items generally determined by radar. This method will be discussed more fully in Section 3.5. No further attempt to determine the aircraft position as a function of time by radar was pursued because of the questionable accuracy and usefulness of such information.

2.8 ESTIMATED ASROC FLIGHT AND SINKING TIME

As the cameras were to be started at launch time, it was not possible to determine the exact flight time of the ASROC missile from the technical photographs. The first frame of Camera No. A-2-6 showed the rocket in the air above the Agerholm, and the splash was seen nine frames later, indicating an approximate time of 27 seconds.

On the motion-picture records, an estimate of the flight time was made by determining the length of the record from the start of the cameras until the splash or to the first visible surface effect. As the cameras at each station were started separately, it was necessary to select records which started at launch time. This was done by observing the length of the smoke plume from the target raft flares on the early portions of the records. Since the flares were started by radio signal at launch time, a short smoke trail on the initial portion of the

photographic record would indicate the camera had started at, or very close to, launch time. On the basis of the photographic records, the flight time is estimated to have been 27 ± 1 seconds.

The sinking time of the weapon was determined from aerial photographs by measuring the interval between the splash and the appearance of surface effects, neglecting the time required for the shock wave to reach the surface (< 0.1 second). This method gave an estimated sinking time of 13.0 ± 0.1 seconds.

TABLE 2.1 CAMERA STATIONS AT THE TIME OF BURST

Station	Type	Location Relative to Surface Zero
A-1A	Aircraft A3D-2P	At an altitude of 20,000 feet, on a 330 degree true heading, 3,200 feet beyond surface zero
A-1B	Aircraft A3D-2P	At an altitude of 20,000 feet, on a 330 degree true heading, 1,100 feet beyond surface zero
A-2C	Aircraft R5D	In a circular flight path at an altitude of 10,000 feet, horizontal range of 31,300 feet, and a true bearing of 150 degrees
A-2D	Aircraft R5D	In a circular flight path at an altitude of 10,000 feet, horizontal range of 35,700 feet, and a true bearing of 250 degrees
S-1	Ship (ATF-106) USS Molala	At a range of 19,100 feet and a true bearing of 338 degrees
S-2	Ship (DD-681) USS Hopewell	At a range of 12,300 feet and a true bearing of 19.5 degrees
S-3	Ship (LSD-35) USS Monticello	At a range of 23,600 feet and a true bearing of 252 degrees

48

TABLE 2.2 CAMERA DATA, STATION A-1A

Camera Number	Camera Type	Film Size	Film Type	Magazine Size	Calibrated Lens Focal Length	Frame Rate (at SZ∏)	Passes Photo-graphed	Timing	Remarks
				feet	mm	ft/sec		cps	
1	Fastax	16mm	Tri-X	400	(50)[1]	(1000)	1	500	Surface Zero not in field of view
2	Milliken	16mm	Plus-X	400	25.83	192	1, 2,	500	
3	KF-8	35mm	Plus-X	1000	18.95	100	1, 2	120	
4	KF-8	35mm	Plus-X	1000	25.50	24	1, 2, 3, 4	120	
5	Cine-Special	16mm	Ektachrome	100	(15)	(24)	1, 2, 3	None	
6	KA-46	5 in	Pan-X	250	152.7	(2)	1, 2, 3	Clock	Aero 2 filter
7	X-70	70mm	Pan-X	50	77.24	(1/8)	1, 2, 3, 4, 5	None	Aero 2 filter
8	CA-13	9 in	Plus-X	370	916.4	(5/8)	1, 2, 3, 4, 5, 6	None	Aero 2 filter
9	KF-8	35mm	Plus-X	1000	(50)	101	1, 2, 3	120	
10	KF-8	35mm	Plus-X	1000	(50)	24	1, 2, 3	120	Camera mounted backwards
11	T-11	9 in	Plus-X	370	(152)	(1/3)	1, 2, 3, 4	Clock	Photographed obliquely; Aero 2 filter

[1] ( ) Indicates nominal value.

49

TABLE 2.3 CAMERA DATA, STATION A-1B

Camera Number	Camera Type	Film Size	Film Type	Magazine Size (feet)	Calibrated Lens Focal Length (mm)	Frame Rate (at 32°F) (fr/sec)	Passes Photographed	Timing (ops)	Remarks
1	Fastax	16mm	Tri-X	400	(50)[1]	(1000)	1	500	Surface Zero not in field of view
2	Milliken	16mm	Plus-X	400	26.19	198	1	500	
3	KF-8	35mm	Plus-X	1000	18.79	99	1	120	
4	KF-8	35mm	Plus-X	1000	25.35	24	1,2,3	120	
5	Cine-Special	16mm	Ektachrome	100	(15)	(24)	--	None	No record, shutter apparently malfunctioned
6	KA-46	5 in	Pan-X	250	152.9	(2)	1,2,3	Clock	Clock did not operate; Aero 2 filter
7	X-70	70mm	Pan-X	50	77.14	(1/8)	1,2,3,4,5,6,7	None	Aero 2 filter
8	CA-13	9 in	Plus-X	370	922.3	(5/8)	1,2,3	None	Used on preshot mapping run; Aero 2 filter
9	KF-8	35mm	Plus-X	1000	(50)	100	1	120	
10	KF-8	35mm	Plus-X	1000	(50)	24	1,2	120	Camera mounted backwards
11	T-11	9 in	Plus-X	370	(152)	(1/3)	1,2	Clock	Photographed obliquely; Aero 2 filter

[1] ( ) Indicates nominal value.

TABLE 2.4 PASSES OF A3D's OVER ARRAY

Pass No.	Time After Burst [1]	Heading	Altitude
		degrees True	feet
		A3D-A	
1	-40 sec	330	20,000
2	1 min 27 sec	098 [2]	19,300
3	4 min 29 sec	193 [2]	10,000
4	9 min	188	10,000
5	23 min	343	10,000
6	30 min	343	10,000
7	49 min	345	10,000
8	55 min	175	5,000
		A3D-B	
1	-40 sec	330	20,000
2	9 min 08 sec	330	20,000
3	15 min 15 sec	169	10,000
4	25 min	335	10,000
5	33 min	165	10,000

[1] Time given refers to start of each pass.

[2] Aircraft was banking.

TABLE 2.5 CAMERA DATA, STATION A-2

Camera Number	Camera Type	Film Size	Film Type	Magazine Size (feet)	Calibrated Lens Focal Length (mm)	Frame Rate (at SZT) (fr/sec)	Approx. Duration of Record (after SZT) (seconds)	Timing (cps)	Remarks
1	Fastax	16mm	Tri-X	400	(100)[1]	(1206)	2.8	500	
2	Milliken	16mm	Plus-X	400	(50)	186	3.5	500	
3	Mitchell	35mm	Plus-X	1000	50.52	105	119	120	
4[2]	Mitchell	35mm	Plus-X	1000	24.80	22	684	120	.
5	Filmo	16mm	Ektachrome	100	(15)	(16)	231	None	
6[2]	P-56	7 in	Plus-X	125	(508)	(1/3)	541	Clock	Clock did not operate, Aero 2 filter
7	P-220	70mm	Pan-X	50	(75)	(1/4)	892	None	Aero 2 filter

[1] ( ) Indicates nominal value.

[2] Located in "D" Aircraft. Unless otherwise noted, cameras were located in "C" Aircraft.

52

TABLE 2.6 CAMERA DATA, STATION S-1

Camera Number	Camera Type	Film Size	Film Type	Magazine Size (feet)	Calibrated Lens Focal Length (mm)	Frame Rate (at SZT) (fb/sec)	Approx. Duration of Record (after SZT) (seconds)	Timing (cps)	Remarks
1	Milliken	16mm	Plus-X	400	50.17	391	27	100	
2	Mitchell	35mm	Plus-X	1000	(100)¹	110	110	120	
3	Mitchell	35mm	Plus-X	1000	(35)	101	127	100	
4²	Mitchell	35mm	Plus-X	1000	(152)	--	--	120	No record, shutter apparently malfunctioned
5	Mitchell	35mm	Plus-X	1000	18.94	30	487	120	
6	Filmo	16mm	Ektachrome	100	(15)	(16)	198	None	
7	F-56	7 in	Plus-X	125	208.8	(1/3)	482	Clock	

1 ( ) Indicates nominal value.

2 Aimed at USS Beusell (DD-845).

53

TABLE 2.7 CAMERA DATA, STATION S-2

Camera Number	Camera Type	Film Size	Film Type	Magazine Size	Calibrated Lens Focal Length	Frame Rate (at SZT)	Approx. Duration of Record (after SZT)	Timing	Remarks
				feet	mm	fr/sec	seconds	cps	
1	Milliken	16mm	Plus-X	200	40.49	171	39	500	
2	Mitchell	35mm	Plus-X	1000	59.09	88	143	120	
3	Mitchell	35mm	Plus-X	1000	24.87	109	107	120	
4	Mitchell	35mm	Plus-X	1000	(25)¹	(48)	280	120	Followed left edge of surge
5	Mitchell	35mm	Plus-X	1000	18.94	21	711	120	
6	Filmo	16mm	Ektachrome	100	(9.5)	(16)	214	None	
7	P-56	7 in	Plus-X	125	210.0	(1/3)	236	Clock	Followed right edge of surge

1 ( ) Indicates nominal value.

54

TABLE 2.8 CAMERA DATA, STATION S-3

Camera Number	Camera Type	Film Size	Film Type	Magazine Size	Calibrated Lens Focal Length	Frame Rate (at 8 M)	Approx. Duration of Record (after 8 M)	Timing	Remarks
				feet	mm	fr/sec	seconds	cps	
1	Milliken	16mm	Plus-X	400	101.32	388	34	100	
2	Mitchell	35mm	Plus-X	1000	(152)$^{\underline{1}}$	--	--	120	No record
3	Mitchell	35mm	Plus-X	1000	50.22	86	274	100	
4	Mitchell	35mm	Plus-X	1000	26.03	50	283	120	
5	Mitchell	35mm	Plus-X	1000	(25)	34	435	120	
6	Filmo	16mm	Ektachrome	1000	(15)	(16)	212	None	
7	F-56	7 in	Plus-X	125	508.5	(1/3)	360	Clock	

1/ ( ) Indicates nominal value.

55

TABLE 2.9   POSITIONS OF THE UPWIND ELEMENTS OF THE ARRAY RELATIVE TO THE
TARGET RAFT AT H-30 MINUTES AND AT THE TIME OF BURST

Object	H-30 Minutes		Time of Burst	
	Range	Bearing	Range	Bearing
	feet	degrees True	feet	degrees True
Splash	--	--	762	128.0
Platform 2 [1]	2226	343.4	2226	343.4
Coracle 3	3275	343.6	3300	343.8
Platform 1	3380	343.6	3390	343.4
Coracle 2	4375	343.1	4425	343.5
Bausell (Stern)	5500	344.0	5590	343.8
Bausell (Bow)	5895	343.4	5975	343.0
Coracle 1	6440	342.9	6550	342.2

[1] Range and bearing determined at time of burst for both times.

TABLE 2.10   POSITIONS OF THE UPWIND ELEMENTS OF THE ARRAY RELATIVE TO
SURFACE ZERO AT THE TIME OF BURST

Object	Range	Bearing
	feet	degrees True
Splash	263	299.0
Target Raft	1045	306.2
Platform 2	3120	332.0
Coracle 3	4180	334.9
Platform 1	4280	334.9
Coracle 2	5314	336.6
Bausell (Stern)	6427	338.2
Bausell (Bow)	6827	337.7
Coracle 1	7426	337.2

TABLE 2.11 POST-SHOT POSITIONS OF UPWIND ELEMENTS OF ARRAY RELATIVE TO STERN OF BAUSELL.

Object	H + 10 Minutes[1]		H + 16 Minutes		H + 30 Minutes	
	Range	Bearing[2]	Range	Bearing	Range	Bearing
	feet	degrees True	feet	degrees True	feet	degrees True
Coracle 1	1012	340.8	1007	334.0	1005	329.5
Bausell (Bow)	386[3]	333.5	394	334.0[4]	387	334.0
Coracle 2	1050	180.5	1080	161.5	1083	161.0
Platform 1	1962	179.2	2104	161.0	2100	160.6
Coracle 3	1976	179.2	2120	161.0	2112	160.4
Platform 2	2020	183.0	2362	162.0	2975	161.0

1. Time is in minutes after the burst.
2. Bearing is in degrees relative to True North.
3. Actual length of Bausell is 390.5 feet.
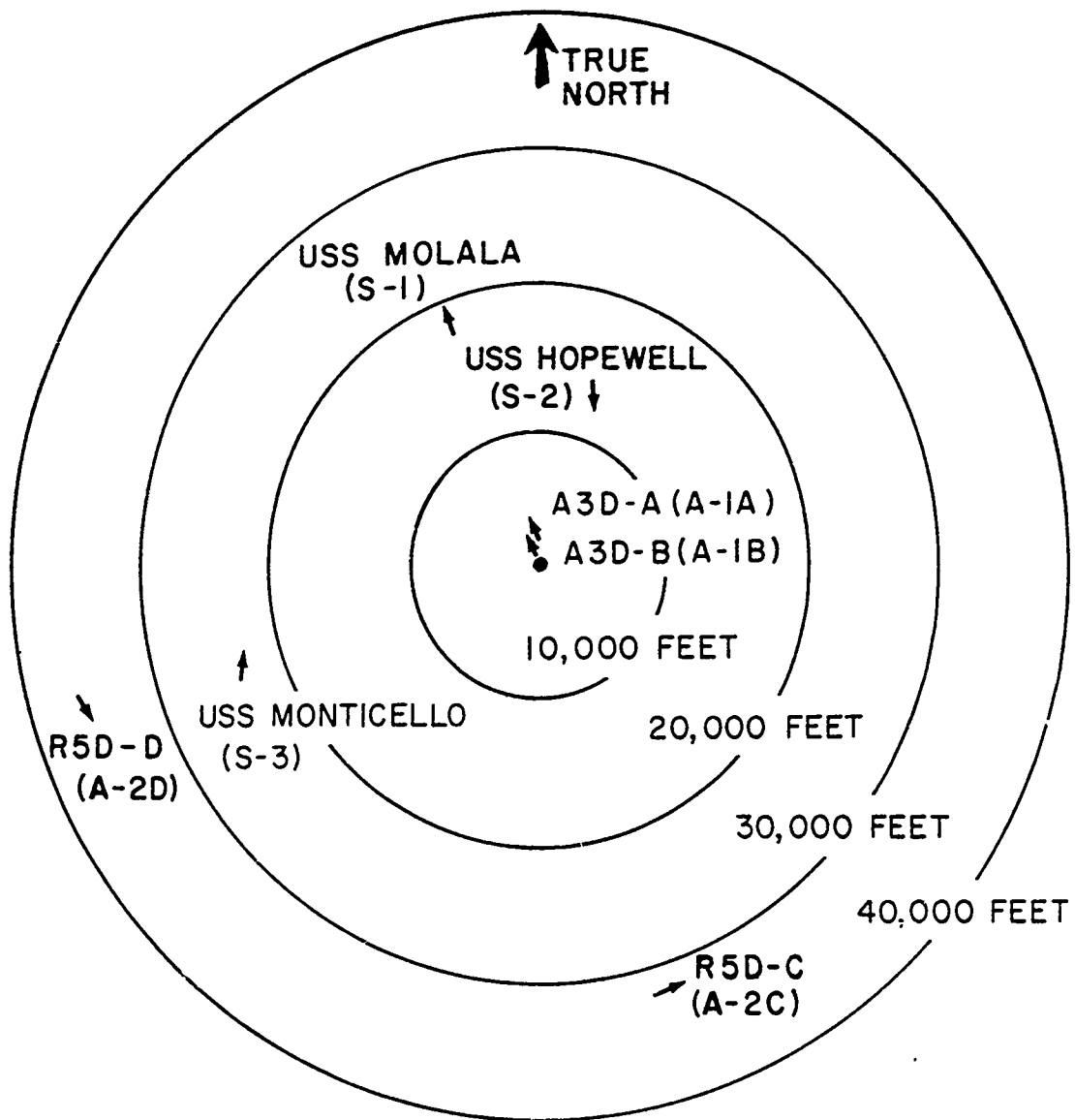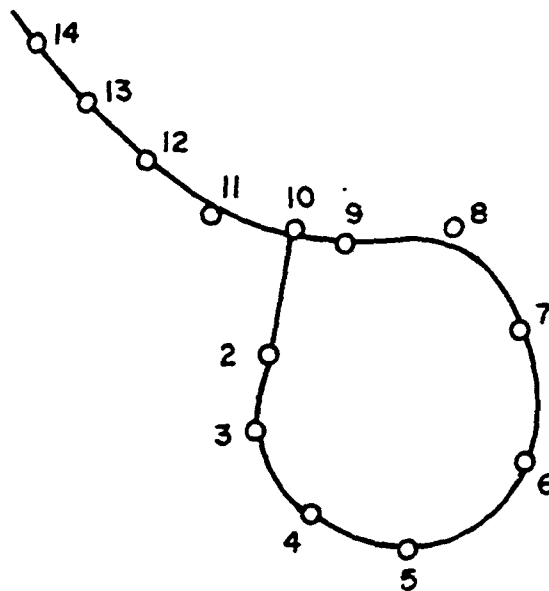4. Photonavigators' records indicate bearing of 338 degrees True for Bausell. Value shown is believed more accurate.

TRUE
NORTH

USS MOLALA
(S-1)

USS HOPEWELL
(S-2)

A3D-A (A-IA)
A3D-B(A-IB)

10,000 FEET

R5D-D
(A-2D)

USS MONTICELLO
(S-3)

20,000 FEET

30,000 FEET

40,000 FEET

R5D-C
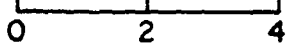(A-2C)

Figure 2.1 Positions of photographic stations at time of burst.

58

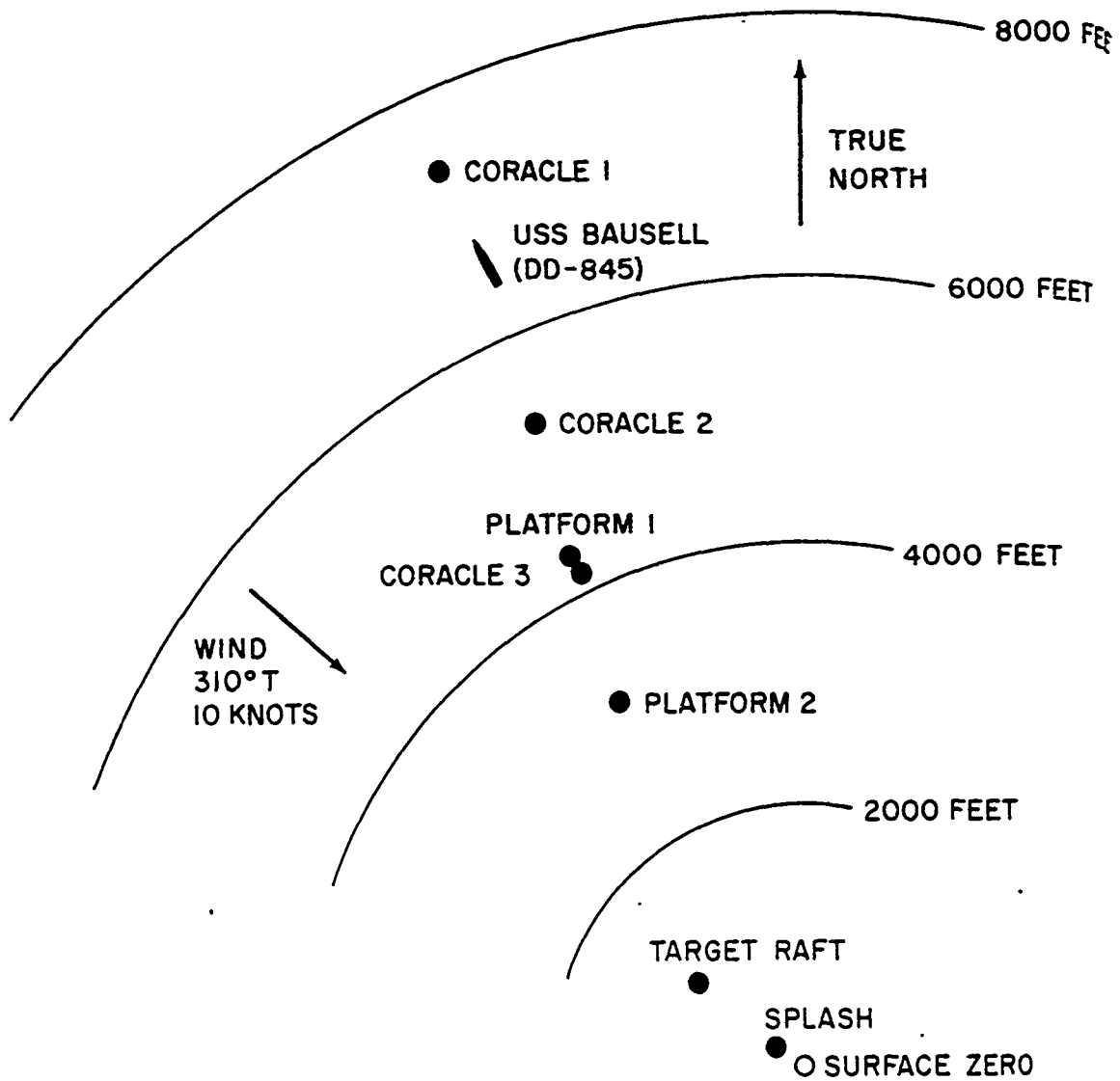Figure 2.2   Motion of Hopewell subsequent to burst.

Figure 2.3 Positions of upwind elements of array at time of burst.

CHAPTER 3
RESULTS

3.1 SPREAD OF UNDERWATER SHOCK WAVES

The first visible surface effect, as seen from the air, was the primary shock-wave slick. This slick appeared as a rapidly expanding dark ring whose outer edge represented the intersection of the primary underwater shock wave with the water surface. The slick had a well-defined edge, which became diffuse as the radius increased. The edge was clearly defined to a radius of 3100 feet and was measurable to a radius of about 4200 feet. Slick radius-vs-time measurements obtained from the two overhead aircraft are presented in Figure 3.1. For comparison purposes a curve for a 680-foot burst depth as predicted by Equation 1.2 is also included in this figure. As slick measurements were also used to estimate the depth of burst, additional measurements and discussion are presented in Section 3.7.

The lateral spread of the spray dome (for a description of the spray dome see Section 1.3.1) followed closely behind the slick for the first 0.2 second [1]. Thereafter, its rate of growth rapidly diminished and the dome reached a maximum radius of 2400 feet at approximately 0.6 second after SZT. This radius represents

---

[1] All times, unless otherwise stated, are in reference to the first visible surface effect. This time is referred to as Surface Zero Time (SZT).

the outer edge of scattered patches of spray. The central spray area, which represents the area of dense spray, continued to expand slowly during the period of measurement. After the slick had travelled outward, a ring of darkened water remained surrounding the dome. This ring had a maximum radial extent of about 3500 feet.

At about 0.66 second after SZT, a cavitation pulse slick and spray ring appeared just outside the extreme edge of the spray dome. This slick and spray ring, which moved rapidly inward toward surface zero, were produced by the collapse of the region of cavitated water. After they had passed, a brightening or intensification of the entire spray dome occurred. The radius of the outer edge of the spray dome also increased at this time.

The appearance and growth of these phenomena are illustrated in Figure 3.2 and are shown graphically in Figure 3.3. Because of the irregular nature of the phenomena and because of the subjectiveness of many of the measurements, considerable scatter occurs in these measurements.

At about 5.3 seconds after SZT a second slick was observed beyond the edge of the spray dome. This slick was not visible in all directions but seemed strongest along a bearing of about 185 degrees True. The second slick was probably produced by the arrival at the water surface of the primary shock wave after it had been reflected by the irregular ocean bottom. No measurements

were made as the slick was too faint and was moving too rapidly to be defined sufficiently.

No bubble-pulse slick was observed on the photographic records. It is doubtful that the slick mentioned in the previous paragraph was produced by the pulsation of the bubble, as such a slick would be symmetrical. In addition, it is possible that a bubble-pulse slick would be obscured by the bottom-reflected slick, as Equation 1.2 predicts that the bottom-reflected slick would reach the outer edge of the dome (a radius of about 3000 feet) at about 5.3 seconds while a bubble-pulse slick would reach this radius about 5.5 seconds after the burst.

The absence of a bubble-pulse slick does not necessarily indicate that the bubble did not pulsate; in fact, plume information indicates definitely that the bubble reached a minimum size and then re-expanded (see Section 3.4). If such a pulsation produced a pressure wave (referred to as a bubble pulse) in the water, the depth at which it was produced may have been sufficiently shallow so that it was weak initially and was rapidly damped in the region of turbulent cavitated water which existed beneath the surface.

3.2 AIR SHOCK WAVES

From the surface camera stations, the first visible evidence of the Sword Fish explosion was the air shock wave resulting from the transmission of a portion of the underwater

63

shock-wave energy across the air-water interface. The shock wave
was visible for about 37 msec before disappearing above surface
zero and was generally visible at other locations for perhaps
100 msec as the underwater shock wave travelled radially outward
from surface zero. Because of the relatively short-focal-length
lenses used, and the lack of fixed reference points in the fields
of view of the cameras, no attempt was made to measure this
phenomenon.

The shrinking and brightening of clouds, produced by the
adiabatic compression and expansion of the air during the passage
of the positive and negative phases of the shock waves, were
observed twice on the color film obtained from the first R5D
(Film No. A-2-5, Station A-2C). No timing was recorded on this
film but visual comparison of the shrinking and brightening with
the surface phenomena indicated that these two shock waves were
the transmitted underwater shock and the shock produced by the
bubble pulsation and subsequent plume emergence. The latter
pulse produced cloud effects which were much more noticeable and
of longer duration, indicating that this shock probably was the
stronger of the two.

3.3 SPRAY DOME

The spray dome appeared almost immediately after the first
air shock wave. The maximum height varied from

64

as measured from the three surface camera stations; this difference in heights was probably due to minor variations in camera distances and the measurement of different jets from different stations. A slight increase in the height of the dome above surface zero was noticed between about 6.5 seconds and the appearance of the primary plumes and possibly was caused by the bubble pulsation. The appearance of the spray dome at various times is shown in Figure 3.4.

The spray dome produced on Sword Fish was one of the smoothest observed on an underwater nuclear burst, probably because of the relatively calm water and because no buoys or floats were located in the vicinity of surface zero. These objects usually produce very high jets, such as occurred on Shot Wahoo (Reference 4). Because the spray dome reached its maximum height before the plumes emerged, it was possible to make a complete study of its growth. The Bausell provided a stable reference point for cameras located on the Molala (Station S-1) and height-vs-time measurements were made at surface zero and at 100-foot intervals left and right of surface zero to a radius of   The height-vs-time curves obtained to the left of surface zero are shown in Figure 3.5. No stable reference point was visible from the other two surface stations; therefore, measurements were made only at surface zero.

As stated in Section 1.3.1, the growth of the spray dome may be described by the following equation:

$$h = V_o t - f t^2 \qquad (3.1)$$

Previously, values of the initial velocity V_o, and the retardation factor f, were obtained by dividing Equation 3.1 through by t. The resulting equation was then a straight line with a Y-intercept of V_o and a slope of f (Reference 4). However, in practice a straight line was not formed through all of the data and an arbitrary decision as to the best linear approximation was made. For Sword Fish, values of V_o and f were obtained by fitting, by the method of least squares, a curve of the form of Equation 3.1 to the height-vs-time data. These values are presented in tabular form in Table 3.1.

At surface zero, an average initial velocity of and an average retardation factor of were obtained. The measured initial velocity was somewhat higher than that predicted by Equation 1.4 for a burst at a depth of 680 feet (see Section 4.1). The occurrence of higher velocities than predicted has been noticed on previous nuclear tests (Reference 5) and also with high explosives. The reason for these consistently higher velocities is only partially understood.

66

The retardation factor at surface zero, as predicted by
Equation 1.8, based on the results of Wahoo, is   The
difference between the predicted and measured Sword Fish
retardation factors is believed to be primarily a result of the
different methods employed in obtaining the Wahoo and Sword Fish
values. As a check, one Wahoo curve was fitted by the method
employed on Sword Fish and a retardation factor consistent
with those measured on Sword Fish was obtained.

Equation 1.9 was solved for different drop sizes with an
initial vertical velocity of   The calculated curves
which overlap the surface-zero spray-dome height-vs-time curve
are presented in Figure 3.6. These indicate a spray-dome drop
diameter between 6 and 7 millimeters. The method is approximate,
because a drop in the dome does not originate at the surface and
is not in free flight in still air. Actual values would there-
fore be less. However, it appears that the spray in the Sword
Fish dome was of the order of raindrop size.

3.4 PLUMES

The primary plumes first appeared on the sides of the spray
dome about 6.3 seconds after SZT. These plumes, which were
produced by the pulsation of the bubble and its subsequent
re-expansion, had risen above the dome and developed into a
roughly hemispherical mass by 7 seconds. The plumes reached a
maximum height of   approximately 16 seconds after SZT and had
a maximum collapsed diameter of 4300 feet at 22 seconds.

67

Extrapolation of the height-vs-time curve down to the water
surface indicated that the time of total central collapse was
about 32 seconds.

The appearance of the primary plumes is illustrated in
Figure 3.7. Height-vs-time and diameter-vs-time curves obtained
from the three surface camera stations are shown in Figures 3.8
and 3.9. Both average and maximum heights are indicated in
Figure 3.8. The maximum height was measured to the extreme top
of the plumes while the average height neglected the spike on
top and was measured across the top of the mass of plumes. The
greater maximum height from Station S-2 resulted from a small
wisp of spray on top of the plumes which was not visible from
the other camera stations. The diameters shown in Figure 3.9
were measured to the extreme edges of the plumes.

Unlike Shot Wahoo, where the horizontal and vertical
components of the initial plume velocity were almost identical
the Sword Fish plumes had a higher vertical than
horizontal component. The vertical component of velocity,
obtained from the maximum height-vs-time curves shown in Figure
3.8, was about   The velocity measured in the
horizontal direction was about   The difference in
velocities indicates that the bubble reached a minimum size
below the water surface and then re-expanded, pushing the water
above the bubble upward and outward in the form of plumes. The

greater vertical velocity occurred because the top of the bubble moved faster than the sides during the re-expansion phase. On Shot Wahoo, the equal components were believed to be a result of the migration of the bubble above the original water surface, leading to equal expansion in both vertical and lateral directions (Reference 4).

As the plumes originated at the time the bubble reached a minimum size, extrapolation of their trajectories back to the origin should give an insight into the time of the minimum, or bubble period, and the approximate depth at which the minimum occurred. The trajectories of twelve plumes were measured; of these, six were considered to be moving in the plane of measurement of the camera and were used in the period determination. Cameras from the S-1 and S-2 stations were used, as these cameras had fixed references in the field of view.

The resulting trajectories and their extrapolations are shown in Figure 3.10. The trajectories were measurable for only a short period of time as the plumes could be followed only after they were clearly defined and until they became obscured by other plumes which were moving toward the camera. In spite of the relatively long extrapolation, these trajectories indicated that the minimum occurred somewhere between 100 and 300 feet beneath the original water surface. Extrapolation of the individual plume height-vs-time curves back to 200 feet beneath the surface

by means of a least-squares fit of the data indicated that the bubble period was

After the primary plumes had settled and the base surge had formed, a second mass of plumes rose above the surge. An illustration of these plumes is included in Figure 3.12. Height-vs-time curves from the three surface camera stations are shown in Figure 3.11. The secondary plumes first appeared about 33 seconds after SZT and reached a maximum height of   about 42 seconds after SZT. They were extremely irregular in shape, with a maximum diameter of from 1700 to 2200 feet being measured from the different stations. It is believed these plumes were produced by the oscillation of the water cavity which had been formed in the water at the time the primary plumes emerged. When the secondary plumes collapsed back to the surface they produced a second base surge within the surge produced by the primary plumes. This second surge is clearly visible on Film No. A-2-7.

The rate of descent of the top of the secondary plumes was about 30 ft/sec as compared with 120 ft/sec for the primary plumes. This is because the top of the secondary plumes broke up into a fine spray prior to settling back.

3.5 VISIBLE BASE SURGE

When the primary plumes collapsed back to the water surface the larger water drops and coherent masses of water dropped into the ocean. The fine drops of spray which had been formed remained

airborne because of their small mass and continued to flow outward radially as a result of the momentum imparted by the expanding plumes. Since the drops entrain air as they move outward, the suspension of drops in air behaves similarly to a dense homogeneous fluid. This dense aerosol is called the base surge.

The base surge formed on Sword Fish is illustrated in Figures 3.12 and 3.13. It can be seen in Figure 3.13 that, because of its cloud-like structure, the surge quickly became difficult to distinguish from the natural clouds and haze on the surface camera records but was readily visible at even later times on the aerial photographs against the water surface background. The base surge was first seen about 14 seconds after SZT. The actual time of appearance varied from station to station and even from different sides of the plumes as observed from the same station. However, until about 22 seconds the surge radius was actually smaller than the plume radius. The surge was visible from the surface camera stations until about two minutes after SZT and patches were visible on the oblique aircraft records until about ten minutes after SZT. Initially the outline of the surge was relatively smooth; however, pronounced lobes soon formed which distorted its toroidal shape. A large lobe formed in approximately the downwind direction, and two lobes formed on the upwind edge of the surge. The upwind portion of the towline lay in a pocket of the surge. Possibly, the surge growth along

71

this line was retarded during its passage over Platforms 1 and 2. Such retardation of the surge by target vessels was observed on both Wahoo and Umbrella (Reference 4).

Measurements of the growth of the surge were made from the three surface camera stations. If the Bausell was visible in the field of view, radius measurements relative to surface zero could be made. On other records, only surge diameters could be obtained. The surge radius-vs-time data are presented in Figure 3.14 and the diameter measurements are presented in Figure 3.15.

At early times, up until about 35 seconds, the measurements from the surface camera stations were probably accurate. However, once the outline of the surge became distorted by the large lobes, the accuracy of the measurements became questionable. The camera-to-subject distance was no longer the distance obtained at the time of burst but depended on the spatial position of the lobe relative to the camera, a value which was almost impossible to obtain. In addition, the surge was being displaced by the wind. The Station S-1 measurements were corrected for the drift of the surge away from the cameras, as this station was upwind of the burst.

The only apparent exceptions to this lobing effect are the measurements obtained from Station S-3. Large lobes formed on the surge almost along the planes of measurement of these cameras and, as it was these lobes which were measured, the camera-to-

subject distance determined at burst time probably remained fairly accurate. This plane of measurement was close to the upwind-downwind axis; therefore these curves probably represent the early growth of the surge in these directions.

The formation and growth of the surge prior to about 25 seconds resulted from the collapse of the smaller plumes and can probably be neglected. At about 25 seconds an acceleration in the surge growth occurred when the large plumes collapsed. For practical purposes, this represents the beginning of the Sword Fish base surge.

The measured heights of the base surge are shown in Figure 3.16. The curves shown were obtained from cameras at Stations S-1 and S-3. As in the radial measurements, the greatest problem in determining base-surge heights was establishing the distance of the highest lobe from the camera. The two camera stations used were separated by an angle of almost 90 degrees. It was therefore often possible to follow the motion of the same lobe from the two stations. Where this was not possible, the motion of the surge toward one station could be estimated from the other.

The crosswind height curve is based on measurements from both stations, taking the highest lobe on the right side as seen from Station S-1 and the highest lobe near the center as seen from Station S-3. The good agreement obtained between these two stations indicated that the same lobe was being measured. The

upwind heights were measured from Station S-1 only, and the distances of the highest points from this station were estimated from Station S-3. The measurements were shifted from one lobe to another or from one peak to another on the same lobe when necessary to obtain the greatest vertical extent of the surge. This was done because the highest parts of the surge tended to evaporate or because surge turrets were rising at different rates. The curves shown in Figure 3.16 were smoothed through the upper limits of the data.

Prior to about 50 seconds, the base surge showed a steadily decreasing height. This probably resulted from the combined collapse of the plumes and formation of the surge. It probably did not represent a true surge height as the surge could not be clearly differentiated from the collapsing plumes. The surge then showed a steady increase in height until it could no longer be measured. However, the rate of rise was relatively slow at 2 minutes. Radioactivity was detected at an altitude of 3000 feet by personnel in the A-2C aircraft when it passed over the foam patch about 15 minutes after the burst. This radiation possibly resulted from the penetration of the surge into the level of the natural clouds. It indicates a continued vertical growth as a result of turbulent diffusion at a rate of about 2 ft/sec.

Because of the lobing of the surge, an accurate outline of its shape could be obtained only from aircraft. A few base-

surge contours were obtained from the Station A-1A aircraft when
it made its second pass over the array; these are presented in
Figure 3.17. Unfortunately, the time interval between passes was
too long to obtain more contours, as the surge was not visible
from directly overhead when this aircraft made its third pass
over the array about 4.5 minutes after the burst. However,
partial contours were obtained by rectifying oblique photographs
from the A-2C and A-2D aircraft. The frames rectified were
from the two films, A-2-6 and A-2-7. Rectifications were limited
to these films largely because of the lack of adequate
resolution of the other cameras at the two R5D stations.

Rectifications were obtained by two means. The analysis
contractor used the Canadian grid method. This technique, which
is described fully in Reference 13, is a graphical method in
which a grid is constructed based on the visible horizon on the
photograph plus the known altitude of the aircraft. The horizon
is used to determine the depression angle and swing angle of the
photograph; the altitude is necessary to correct for the elevation
of the camera. The grid is analagous to a set of railroad tracks
which appear to meet at the horizon. This grid is overlaid on
the photograph, and the coordinates of various points (such as the
base surge, foam patch, and fixed objects) are determined. These
coordinates are plotted in a rectangular grid system, which is
then overlaid on a master plot containing the known positions

of various objects (such as the towed array and ship positions in the case of Sword Fish). This is necessary to check the accuracy of the resulting rectification, to determine the relationship of the plot to True North, and also quite often to locate surface zero, which is not visible or cannot be determined accurately on the photograph itself.

The Canadian grid method worked quite well for Film No. A-2-7; however, no horizon was visible on Film No. A-2-6. Therefore, an alternate method was devised at NOL to rectify photographs from this film (Reference 14). This method describes mathematically the projection of a rectangular grid system on the oblique photograph, similar to the Canadian grid, thus enabling use of an electronic computer. By assuming various depression angles and comparing the resultant ship positions with their actual positions, the correct angle for use in obtaining the surge contours was determined. Where insufficient photogrammetric control was available, it was often possible to determine the correct depression angle by use of the foam patch. As the foam patch was approximately circular, these photographs were rectified to obtain a circular foam patch contour whose center and the few known objects agreed with the master plot of surface zero and the ship positions. While the method is bootstrap in nature, consistent results were obtained.

The accuracy of both methods depended entirely on the
accuracy of the locations of the ships in the area. Fortunately,
there were several ships, and their positions as reported in
Reference 1 were known with sufficient accuracy, the only
exception being the position of the Hopewell. The Hopewell's position
at or shortly after the burst was accurate; however, by three
minutes after the burst considerable disagreement between the
positions obtained on the rectifications and the reported
positions was noted. The Hopewell was not used as a reference
point beyond this time. The ship positions most often used were
those of the Bausell, Anderson, Agerholm, Preston, Molala, and
Monticello. These ships (except for the Monticello) were
located in approximately the upwind direction so that, when the
aircraft was downwind of the burst, the ships often appeared
bunched in the upper portion of the photographs. Because the grid
becomes so sensitive to error as the horizon is approached, it was
generally impossible to rectify these frames.

The resulting partial contours of the surge and foam patch
are presented in Figures 3.18A, 3.18B, 3.18C, and 3.18D. The
accuracy of these contours is believed to be about ± 500 feet,
the uncertainty being due to the doubt concerning the depression
angles and the location of surface zero. It was not attempted to
obtain complete foam patch contours on all the rectifications.
In most cases, only a sufficient number of points was obtained

to get a general outline of the patch. Where this was done, only the data points have been indicated.

The contours obtained by this method are adequate for obtaining overall outlines of the surge; however, the method does not give every detail of the surge. This is especially true of indentations and inner dimensions of the surge. The pockets in the surge were obscured by the body of the surge itself; however, the inner edge on the opposite side of the surge, if well defined, could probably be obtained. On Sword Fish, the collapse of the secondary plumes produced a second surge which, though visible, did not have an edge sharp enough for measurement. However, it obscured the inner edge of-the main surge. The oblique photographs apparently have the advantage over the vertical photographs in the duration in which the surge is visible, as it was still seen six minutes after the burst on the obliques, while it could not be seen from overhead at 4.5 minutes.

The upwind, downwind, and crosswind extent of the surge are shown in Figure 3.19. Up to 100 seconds, the radial curves measured from Station S-3 were used for the upwind and downwind extent. The crosswind extent up to about 35 seconds was taken from the diameter measurements in Figure 3.15. Beyond these times, the curves were based on the partial contours. Measurements on the contours were made to the extremes of the surge in these directions. The smoothed curves shown in Figure 3.19 tend to

78

favor the maximum values. The upwind extent is open to conjecture because the surge was well dissipated by the time the aircraft were in position to photograph this extent, and only a few points were obtained. Also, the contours at late times may not be accurate because of the difficulty in determining the edge of the surge. However, they definitely indicate a continued increase of the crosswind extent of the surge until this time.

The initial radial velocity of the surge was about 115 ft/sec. By 100 seconds, the rate of growth shown by the crosswind curve had diminished to about 20 ft/sec. The growth in the downwind direction was about 40 ft/sec, and in the upwind direction it was about 15 ft/sec at this time. At 150 seconds after SZT the crosswind growth had reached a velocity of 15 ft/sec, which remained approximately constant for the remaining period of measurement. The downwind growth had reached a constant velocity of 33 ft/sec at this time, while the growth in the upwind direction had ceased. It is interesting to note that at this time the difference in velocities between the crosswind and downwind curves was almost exactly that of the wind speed, which was about 10 knots or 17 ft/sec.

3.6 FOAM PATCH

As the base surge expanded and drifted downwind, a white, roughly circular area could be seen on the water surface surrounding surface zero. This area, referred to as the foam

patch, probably consisted of foam, debris, and spray churned up by the violent action of the explosion. The appearance of the foam patch is illustrated in Figure 3.20.

The patch gradually lost its whiteness until, about 17 minutes after the burst, only a white fringe remained on the edge. Besides its white appearance, the foam patch at later times was also distinguishable by a distinct change in wave pattern. The wave pattern within the patch was very irregular while that outside was relatively regular. This demarcation was especially visible from overhead at about 10 and 17 minutes after the burst.

The foam patch probably represented the region of contaminated water. Project 2.1 noted a large increase in radiation when it attempted to enter the patch about 20 minutes after the burst (Reference 11).

Measurements of the growth of the foam patch up to ten minutes after the burst are shown in Figure 3.21. These measurements were obtained from the contours shown in Figures 3.17 and 3.18, and from the second pass of the A-1B aircraft over the burst about nine minutes after the burst. No measurements could be made beyond this time as the passes of the two A3D's were made at lower altitudes (10,000 feet or less), and the dimensions of the foam patch exceeded the fields of view of the cameras.

The foam patch showed a continued growth during the period of measurement. As no distinct drift or increase in size along any one diameter was apparent, an average curve has been drawn through the measured diameters. Two large lobes formed on either side on the 115- to 295-degree axis. Initially, these were very distinct; however, their growth rapidly levelled off, and they probably eventually merged with the main body of the foam patch. The diameter measured across these lobes is shown as a dashed line in Figure 3.21. Scattered patches of foam, primarily on the downwind edge of the patch, were still visible when the last photographic record was obtained about one hour after the burst.

3.7 DETERMINATION OF YIELD AND DEPTH OF BURST

One of the objectives of Project 1.2 was to estimate, by means of surface-phenomena measurements, the yield and depth of burst of Sword Fish. Three phenomena may be used for the determinations: the spread of the primary shock-wave slick; the initial velocity of the spray dome; and the bubble period as determined from plume trajectories. The slick provides the best means of estimating the depth of burst, as it is practically independent of yield, and accurate measurements can easily be obtained. The ratio of the spray-dome velocity at a point on the dome to velocity at surface zero is also independent of yield and can be used to estimate the depth of burst. Spray-dome velocities

81

and the bubble period are dependent on both yield and depth of burst; however, of necessity they were used to estimate the yield in the case of Sword Fish.

Generally, several measurements of each phenomenon were used to estimate the yield or depth of burst. The values given in this section are arithmetic means, and the deviation from the mean is expressed as the standard deviation of a single observation, defined as (Reference 15):

$$\sigma = \sqrt{\frac{\Sigma (x - \bar{x})^2}{N - 1}} \qquad (3.2)$$

Where:

σ = standard deviation of a single observation

N = number of observations

x = single observation

$\bar{x}$ = arithmetic mean

If data have a Gaussian distribution, about 68 percent of all the observations will fall between $\bar{x} + \sigma$ and $\bar{x} - \sigma$ and about 95 percent will fall between $\bar{x} + 2\sigma$ and $\bar{x} - 2\sigma$.

3.7.1 Depth of Burst from Slick Measurements. The measurement of the spread of the underwater shock-wave slick along the water surface has become a standard method for estimating the depth of underwater explosions. Equation 1.2 has been used to estimate the growth of this slick for a given depth. However, this equation

assumes a constant shock-wave velocity, which is not strictly correct. At positions close to the explosion the velocity is very high and is dependent on the yield, while at greater distances the effect of the temperature gradients in the water becomes important. Project 1.1 has accounted for this yield dependency and varying velocity in Reference 12 and has computed the arrival time of the underwater shock wave at various positions, including positions at the water surface. The computed arrival times at the surface were used in determining the depth of burst from slick measurements.

Measurements obtained from three cameras were used in this determination. It had been intended to use the Fastax records from the two overhead aircraft; however, surface zero was out of the field of view of these cameras. The three cameras utilized were also located in the two A3D's and were selected because of their resolution and speed. Smooth curves were drawn through the measured radius-vs-time values obtained from each camera, and arrival times of the slick were determined at 500-foot intervals for radii from 1000 to 3000 feet. The determination of the depth of burst was limited to this region because at smaller radii small timing errors would grossly affect any depth determination, and at radii greater than 3000 feet the measurements showed considerable scatter because of the diffuse nature of the slick.

The arrival times and calculated depths of burst are tabulated in Table 3.2. Based on slick measurements, the depth of burst for Sword Fish was estimated to be 680 (± 20) feet.

3.7.2 Depth of Burst from Spray-Dome Velocity Ratios. The ratio of the initial spray-dome velocity at any point along the surface to that at surface zero is independent of yield and thus can be used to estimate the depth of burst. The relationship between these ratios and the depth of burst is given by Equation 1.5 and is shown graphically in Figure 3.22. The measured ratios are also included in this figure, and the ratios and resultant depths of burst are tabulated in Table 3.3. Based on this method, the Sword Fish depth of burst was estimated to be 710 (± 40) feet.

While this method is useful if no slick measurements are available, it gives only an approximate depth. The difficulties in using the spray-dome ratios are: (1) at positions close to surface zero, the ratio is so insensitive to depth that no realistic value can be determined; and (2) at large distances from surface zero it is difficult to determine the small spray-dome velocities accurately.

3.7.3 Yield from Spray-Dome Velocities. The initial velocity of the spray dome is related to the peak pressure in the underwater shock wave and thus to the yield. Equations 1.1 and 1.4 can be used to determine the yield if the depth of burst is known. The theoretical curves of initial velocity as a function of yield for

84

a 680-foot burst depth are shown in Figure 3.23. Average values of the initial velocities obtained from the three surface camera stations, as reported in Section 3.3 and tabulated in Table 3.1, were used to estimate the yield. These values are also shown in Figure 3.23.

At surface zero, a yield of ⁻   is indicated by spray-dome velocities for an assumed 680-foot burst depth. However, the uncertainty in burst depth increases the possible spread in yield. Including this uncertainty gives a yield estimate of

              . kt. Thus, a scatter of 4.3 percent in spray-dome velocity plus a scatter of 2.9 percent in burst depth produced a yield estimate with a possible accuracy of 20 percent.

It is known that higher spray-dome velocities than predicted by Equation 1.4 are generally produced. The reason for this is not completely understood; however, it seems likely that the yield estimate determined by this method is high. In addition, higher yields are generally indicated at increasing radial distance from surface zero (Reference 4), although such a trend is not as noticeable for Sword Fish. Therefore, the yield determined by this method should be used only as an indication and should not be considered the actual yield of Sword Fish.

3.7.4 Yield from Bubble Period. A measurement of the bubble period may be used to calculate either the depth of burst or the yield of an underwater explosion by means of Equation 1.12. As

the slick provides a good estimate of the burst depth and is almost
independent of yield, the measured bubble period is most useful
in estimating the yield. As reported in Section 3.4, a bubble
period of   was obtained by extrapolating plume
trajectories back to their origin.

The variation in period as a function of depth of burst for
various yields is shown in Figure 3.24. For a 680-foot burst
depth, a yield of   was obtained. If the
uncertainty in depth is included, the possible range is increased
to   Thus a scatter of 6.2 percent in the period
measurement plus 2.9 percent in the burst depth produce a yield
estimate with an accuracy of   This is due largely to
the insensitivity of Equation 1.12 to the yield.

If the yield is known, the bubble period can be used to
estimate the depth of burst. Assuming a   yield, the depth
of burst from the measured Sword Fish bubble period is 670
(± 60) feet.

3.7.5 Recommended Yield and Depth of Burst. Consistent
depth-of-burst estimates were obtained from the various surface-
phenomena measurements. These estimates are also consistent with
the preliminary burst depth of 670 feet determined by Project 1.1
(Reference 12). The slick is practically independent of yield,
and the smallest deviation from the mean was obtained using this
phenomenon. Therefore, the burst depth of 680 (± 20) feet

86

obtained from the slick measurements probably represents the best estimate based on surface phenomena.

No consistent yield estimate was obtained. The yield estimated from the measured bubble period was consistent with the radiochemical yield of ___ (Reference 11) and with the preliminary yield of ___ obtained by Project 1.1. The yield obtained from spray-dome measurements was somewhat higher than that from other sources; however, this was expected, as the spray-dome technique is not always reliable. The relative insensitivity of surface phenomena to yield makes it difficult to obtain precise estimates. Therefore, the yields obtained by other projects should be given greater weight in the determination of an official value for Sword Fish.

Page 88 Deleted

TABLE 3.2 DEPTH OF BURST FROM SLICK MEASUREMENTS

Film No.	Slick Radius	Arrival Time	Depth of Burst
	feet	seconds	feet
A-1A-2	1000	0.104	675
	1500	0.190	690
	2000	0.283	685
	2500	0.377	705
	3000	0.473	715
A-1A-9	1000	0.108	645
	1500	0.193	670
	2000	0.285	660
	2500	0.380	680
A-1B-9	1000	0.105	675
	1500	0.191	660
	2000	0.282	690
	2500	0.378	700

Mean Depth of Burst: 680 feet
Standard Deviation :   ± 20 feet

TABLE 3.3   YIELD AND DEPTH OF BURST FROM INITIAL SPRAY-DOME VELOCITIES
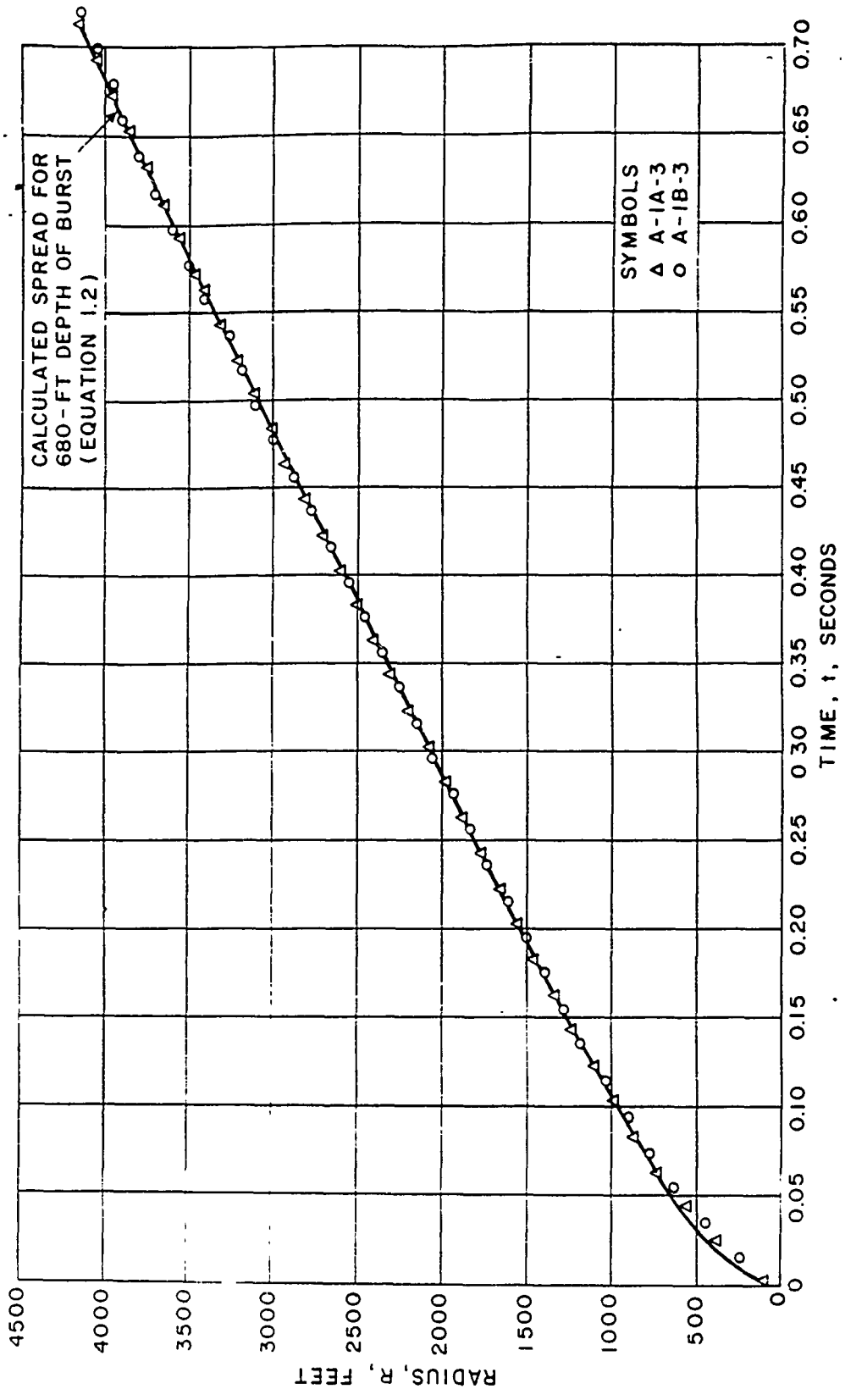
Figure 3.1 Spread of underwater shock-wave slick along the water surface.

0.17 SECONDS

0.70 SECONDS   FILM NO. A-IB-8
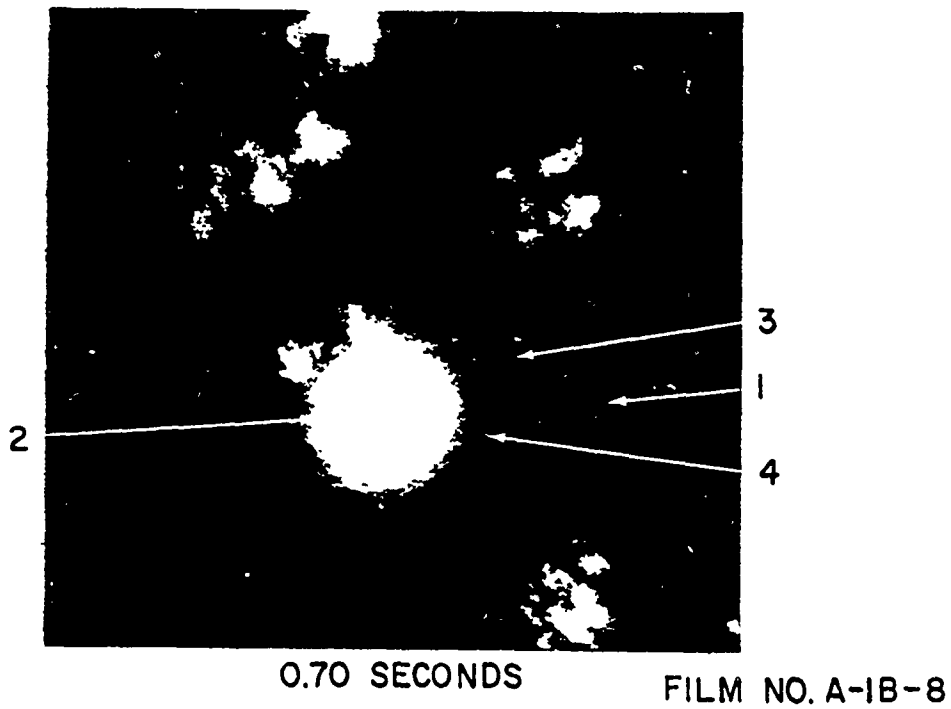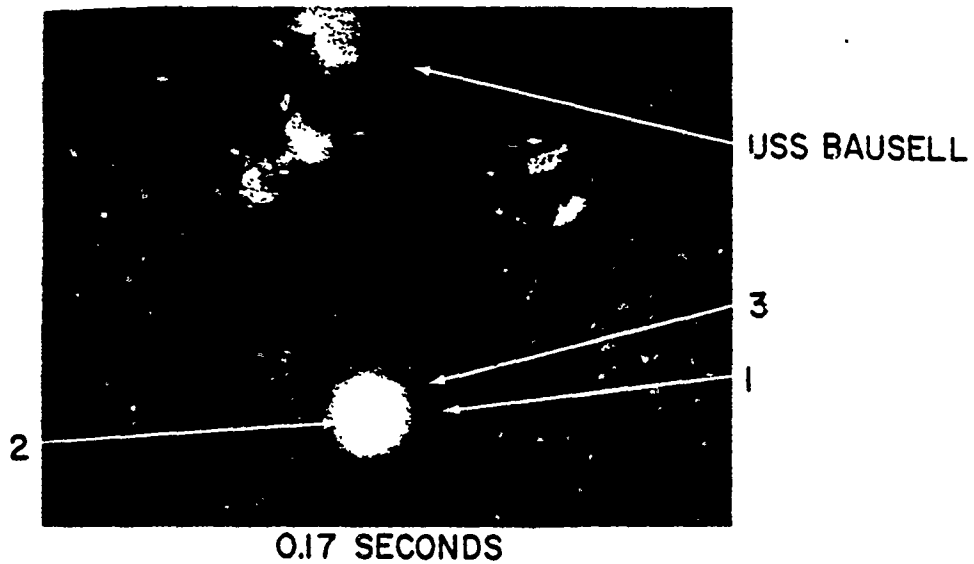
1 PRIMARY SHOCK WAVE SLICK
2 CENTRAL SPRAY AREA
3 OUTER EDGE OF SPRAY DOME
4 CAVITATION PULSE SPRAY RING

Figure 3.2 Slick and spray-dome phenomena as seen from the air.
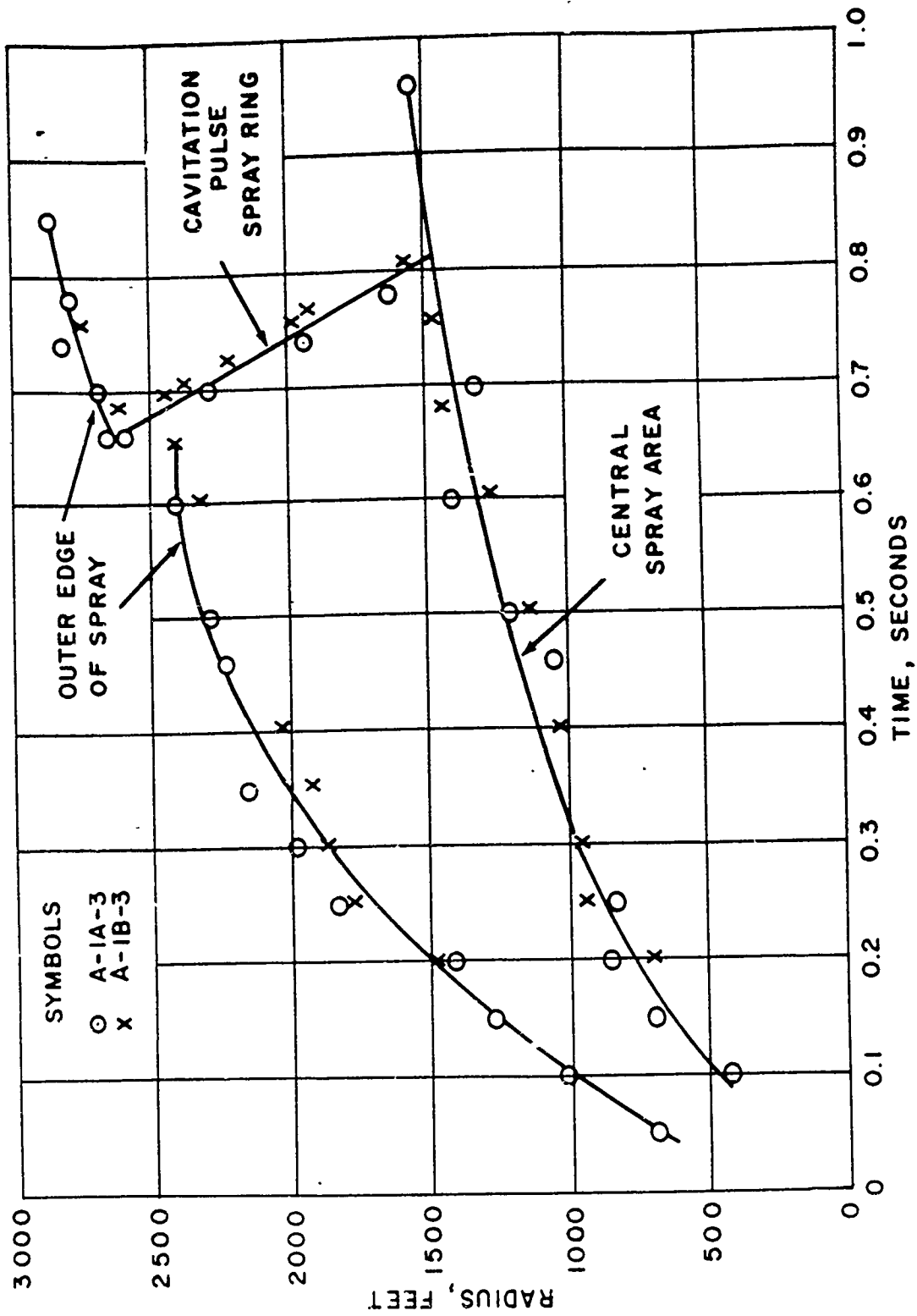
Figure 3.3 Lateral spread of spray dome and spray ring.
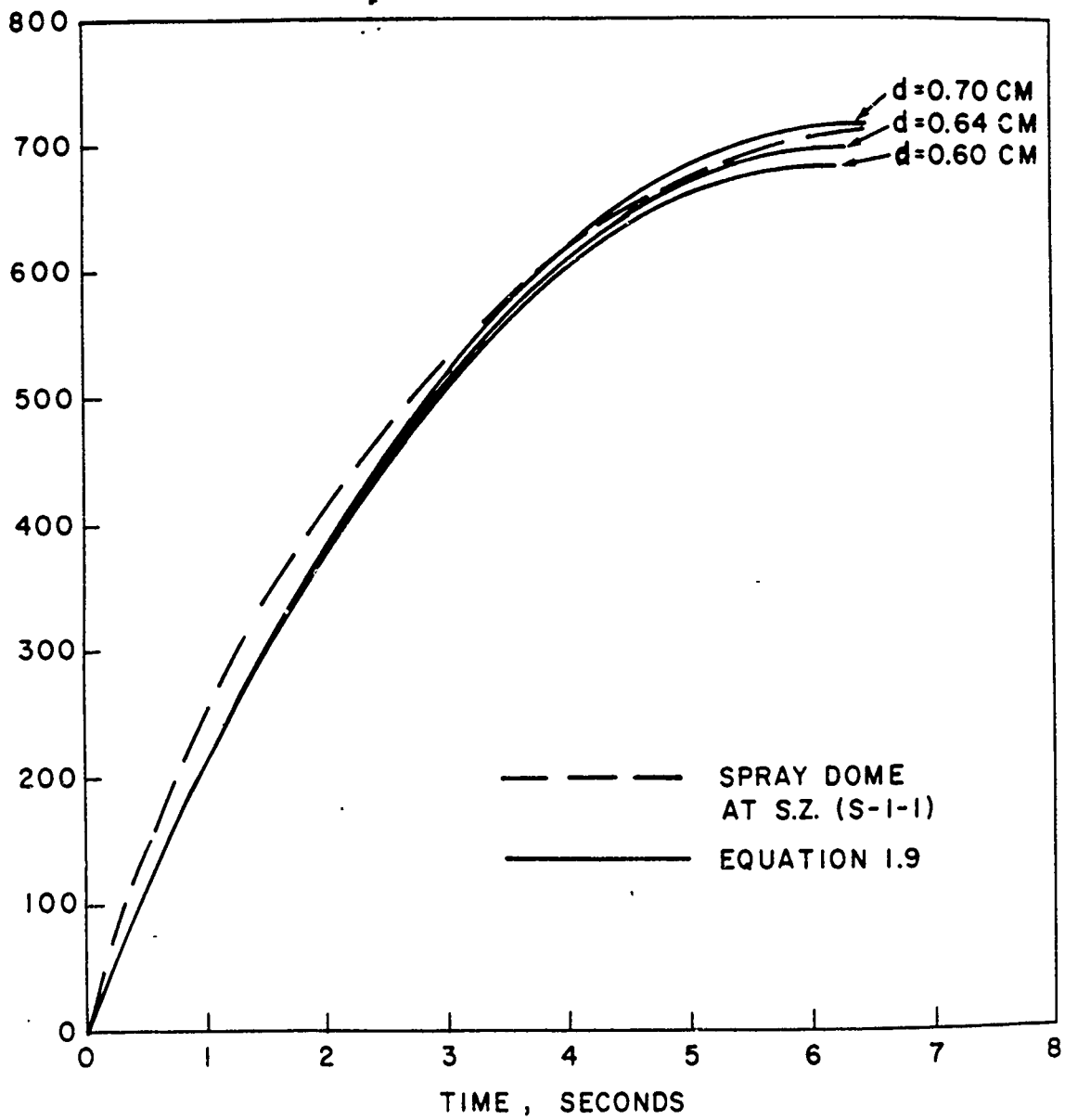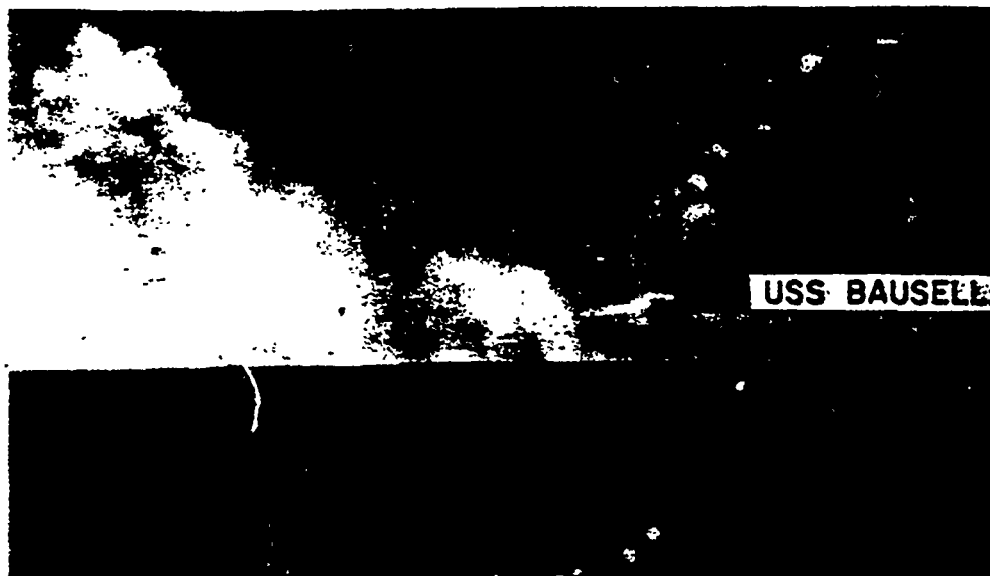
92

Page 93 ~ 94
Deleted

Figure 3.6 Comparison of rise of spray dome with
water drop height-versus-time curves.

Pages 96-97-98-99-100-101 Deleted.

95

87 SECONDS

FILM S-2-7

III SECONDS

FILM A-2-6

Figure 3.13 Base surge and foam patch at late times.
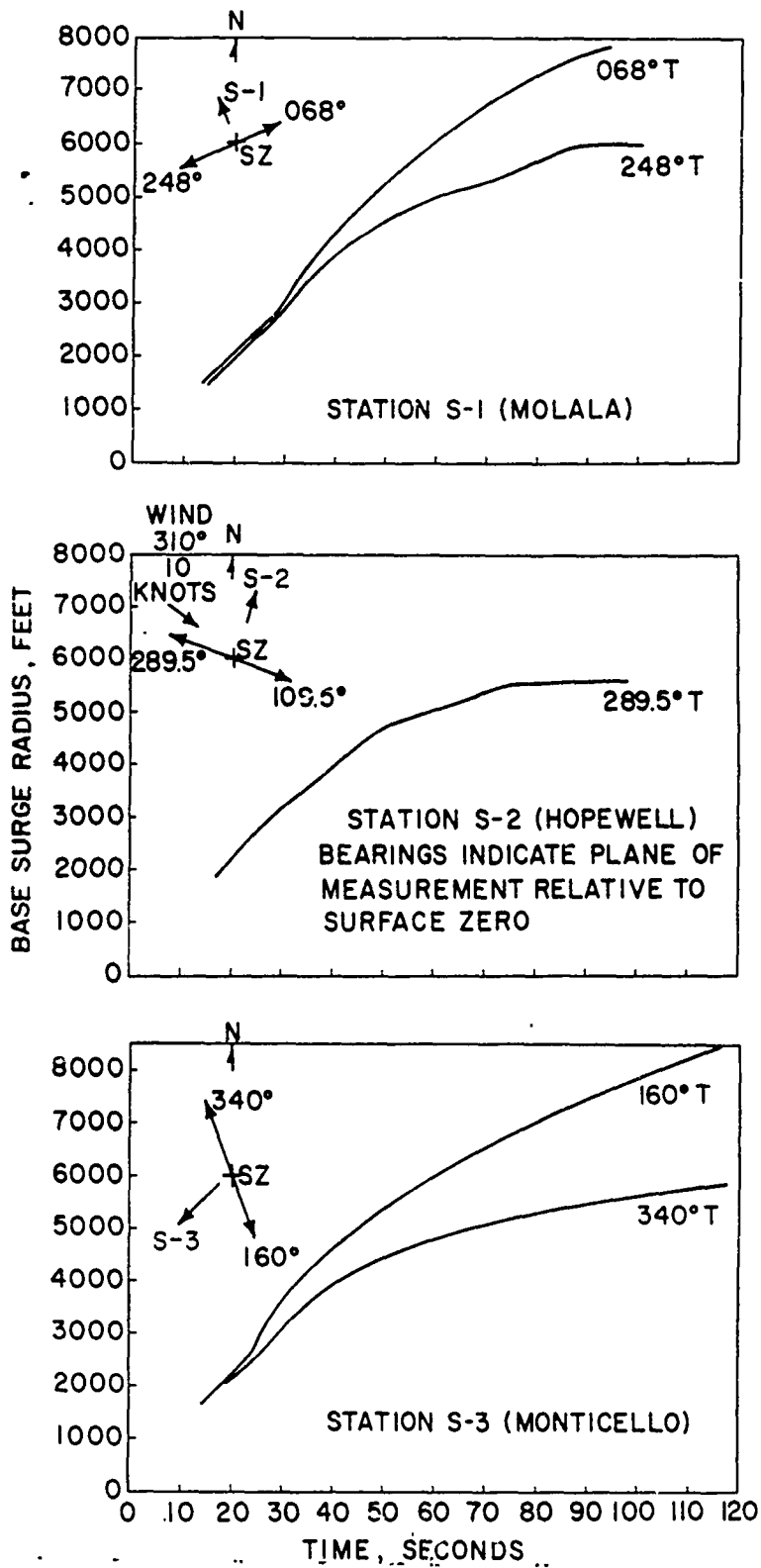
Figure 3.14 Base-surge radial growth measured
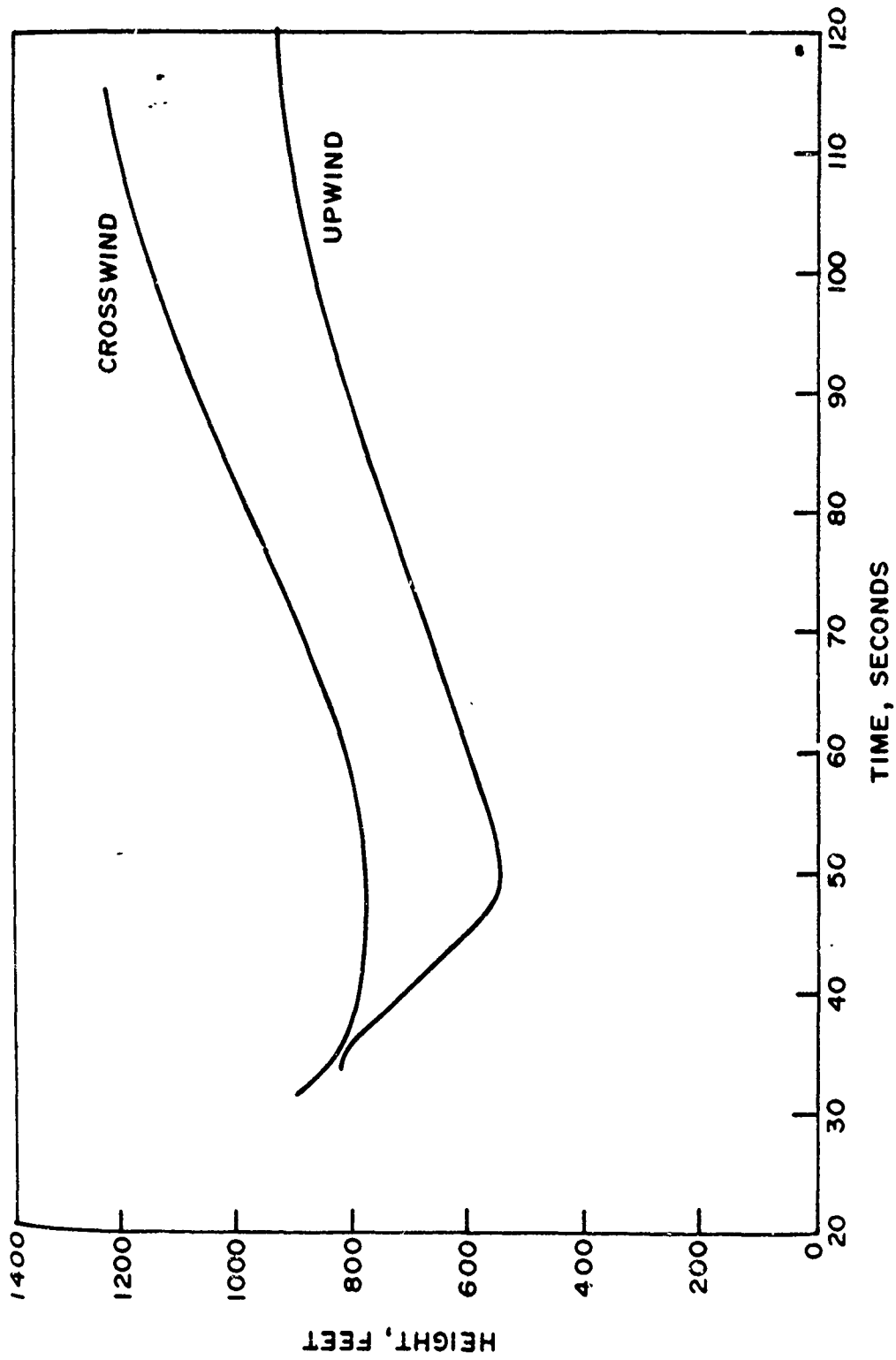from surface camera stations.
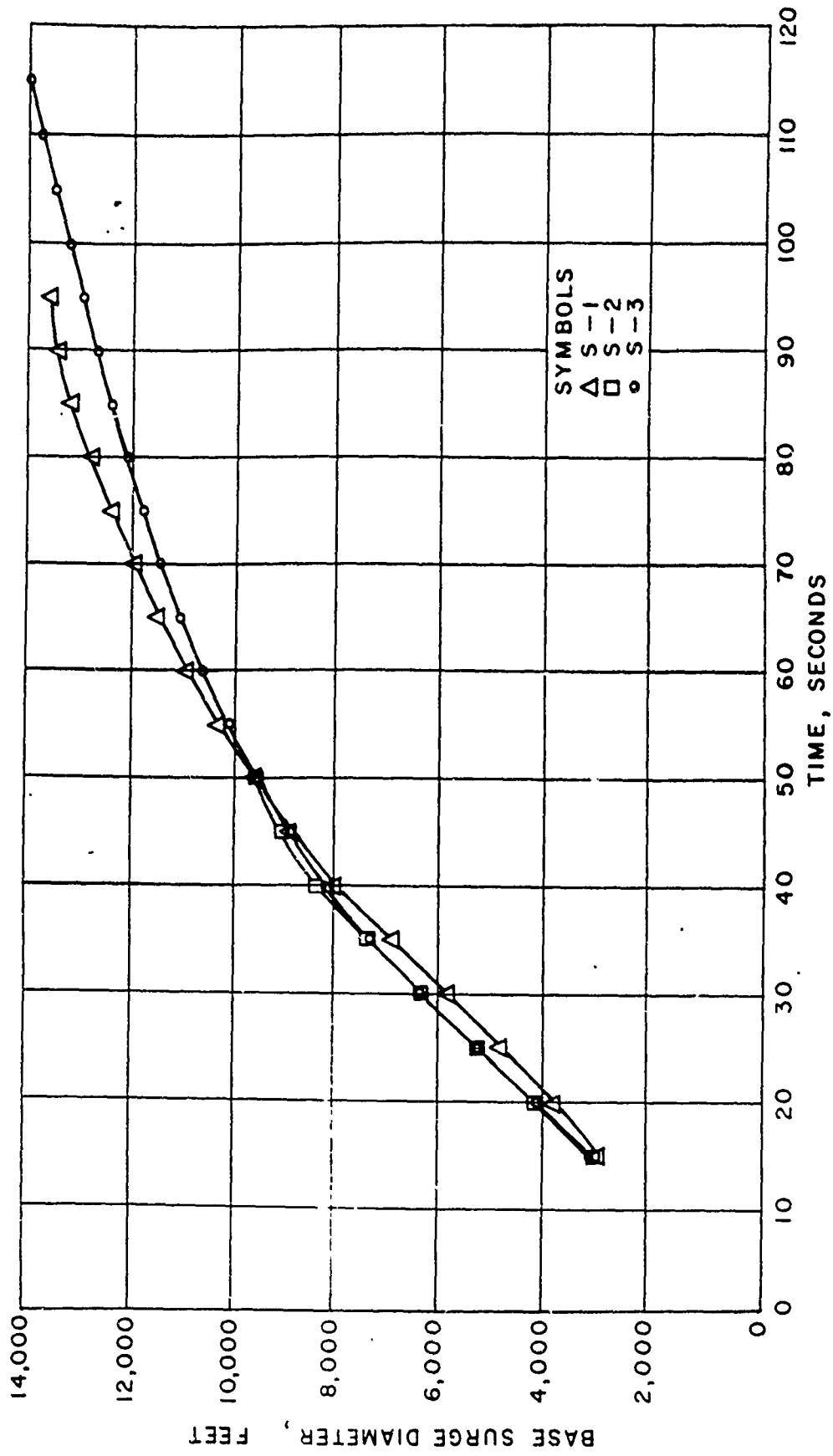
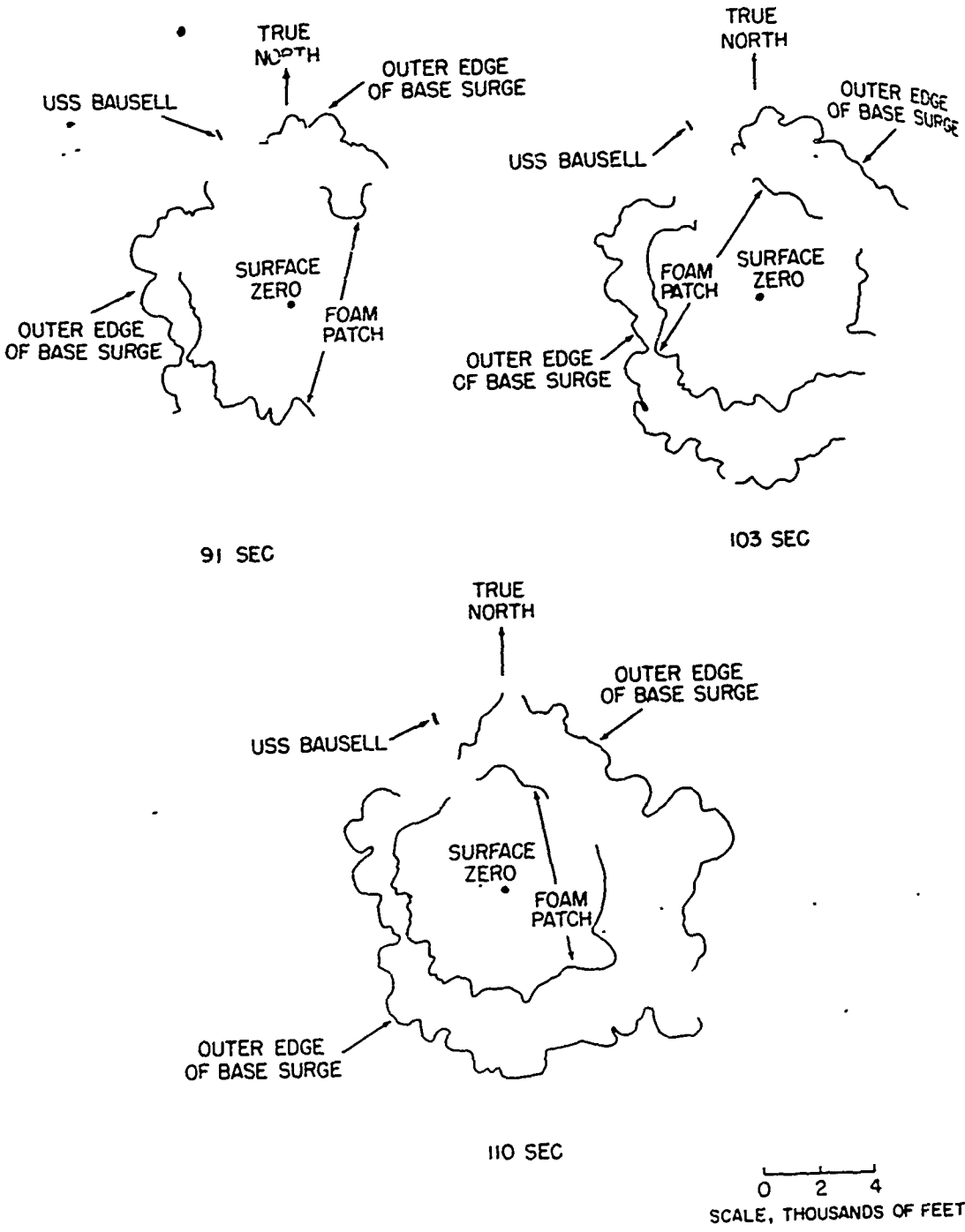Figure 3.15 Base-surge diameters.

Figure 3.15 Base-surge heights.

105

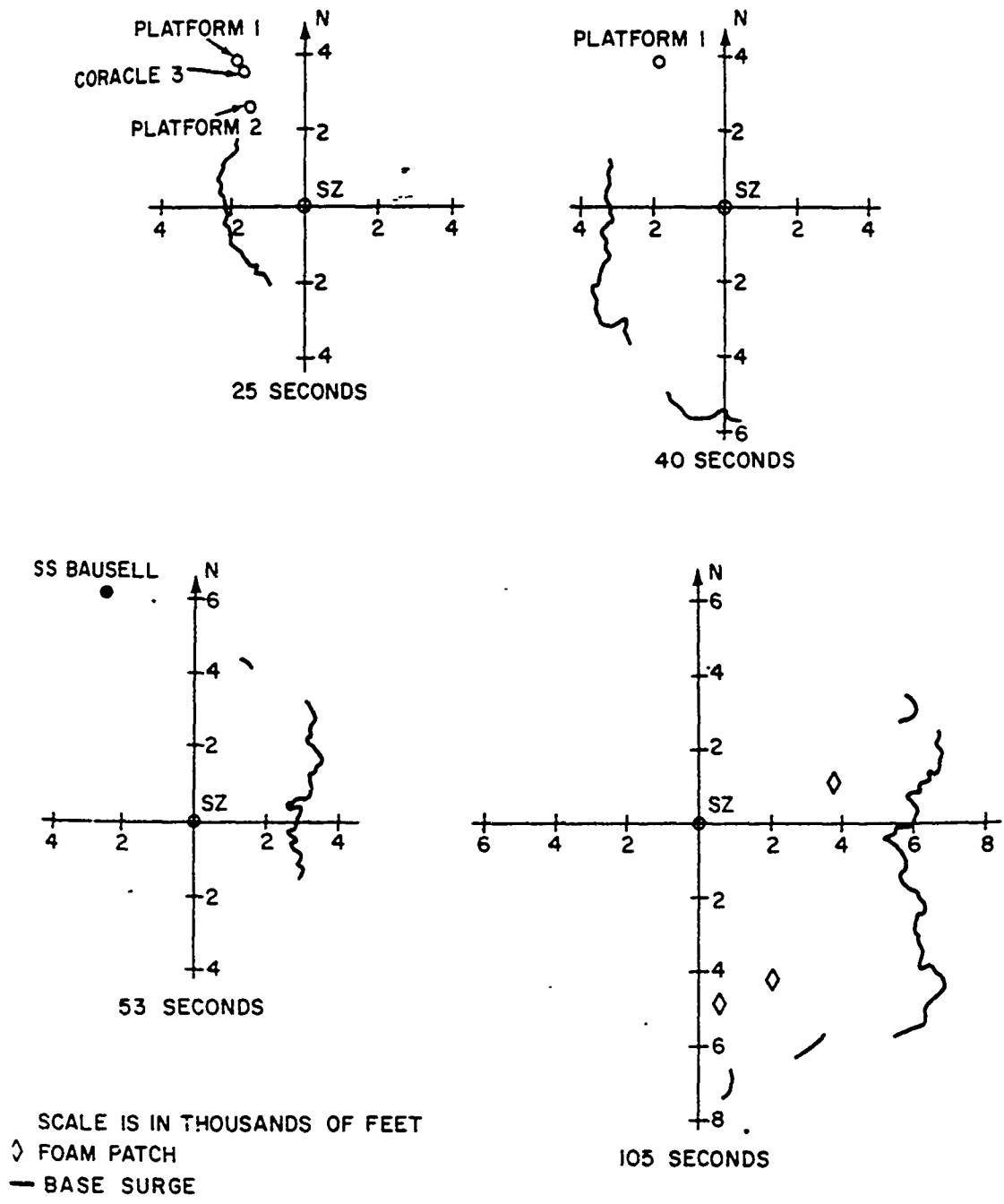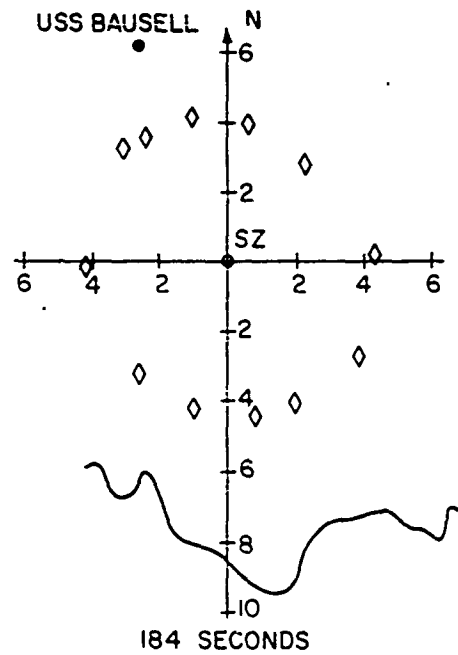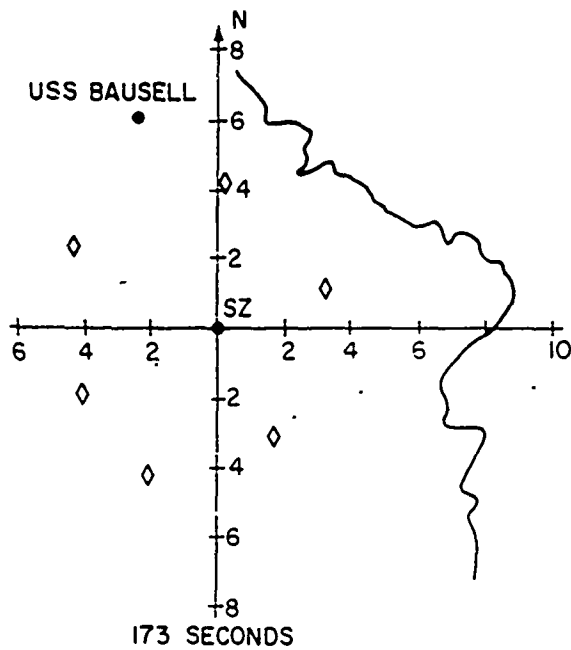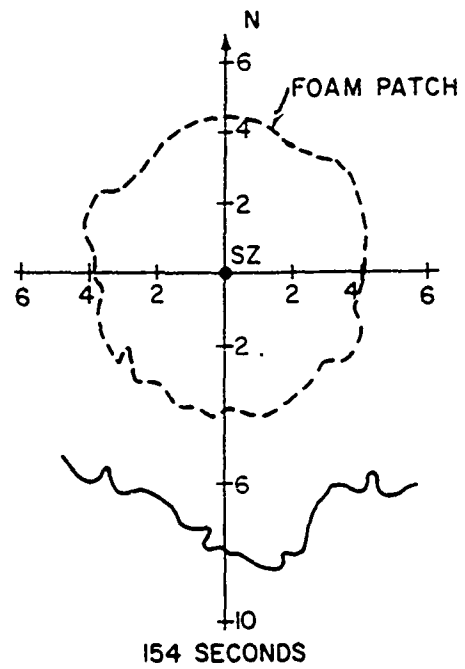Figure 3.17 Base-surge and foam-patch contours from overhead aircraft.

106

Figure 3.18A Base-surge and foam-patch contours, at
25, 40, 53 and 105 seconds.
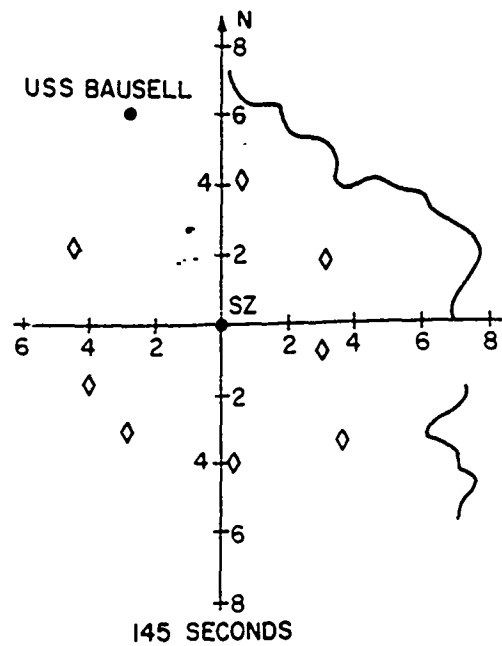
Figure 3.18B Base-surge and foam-patch contours, at 145, 154, 173 and 184 seconds.
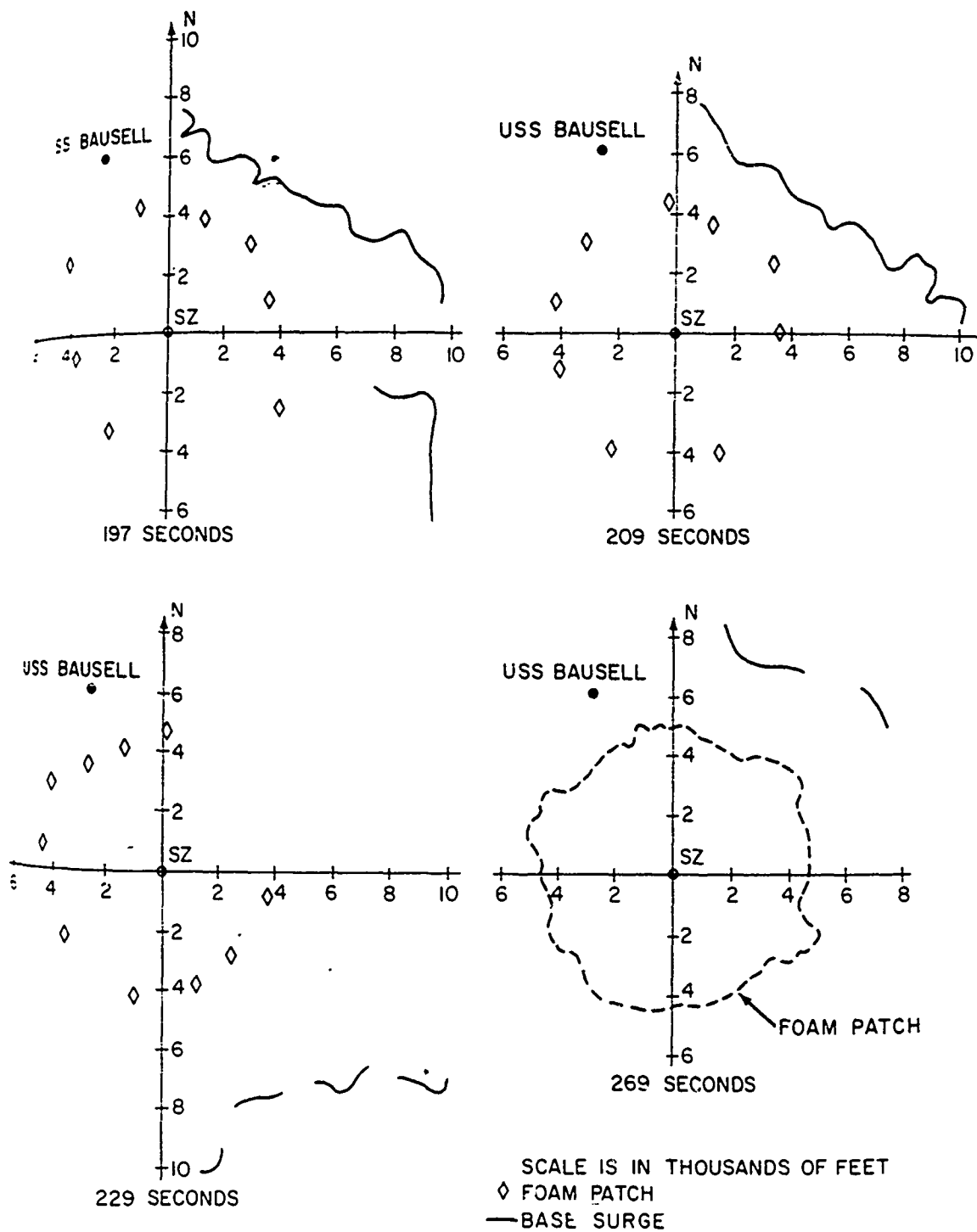
Figure 3.18C Base-surge and foam-patch contours, at
197, 209, 229 and 269 seconds.

109
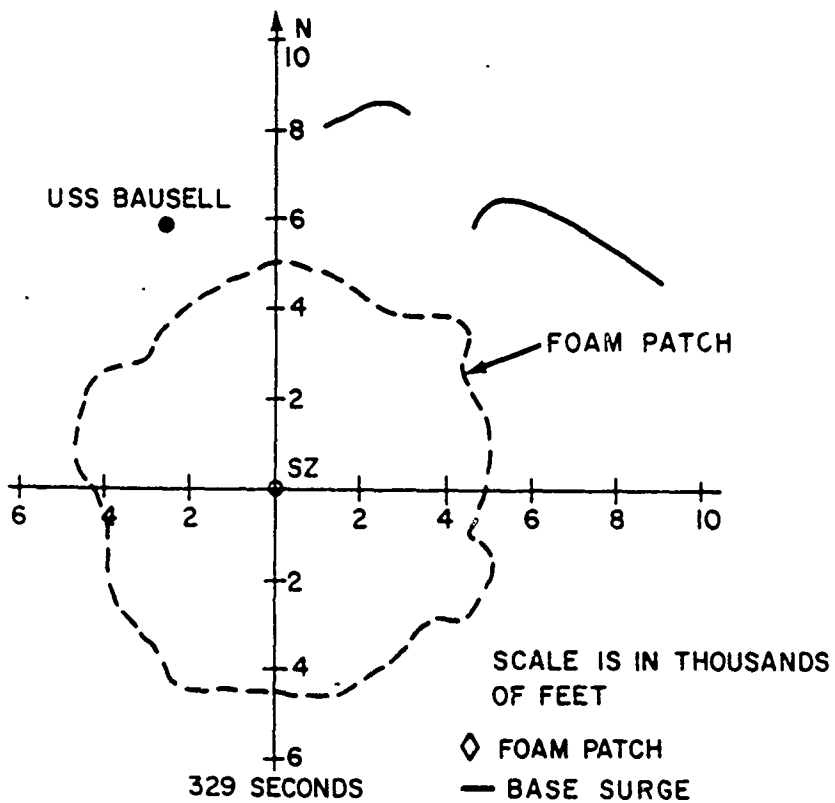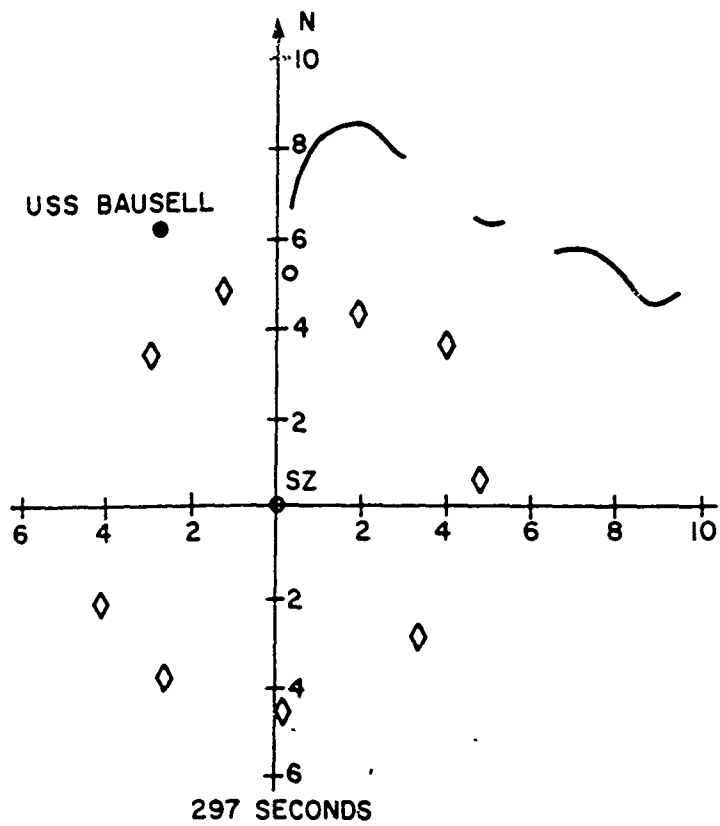
Figure 3.18D Base-surge and foam-patch contours,
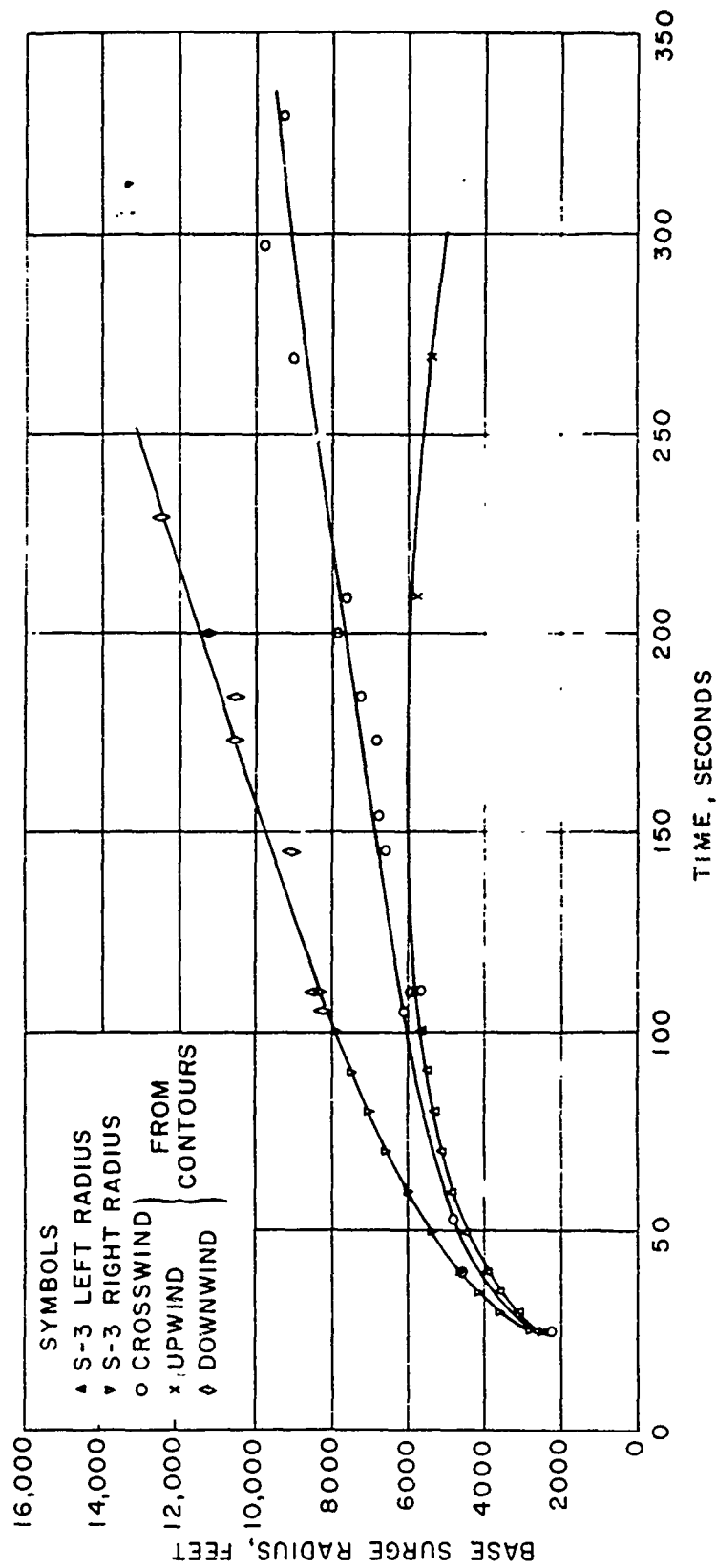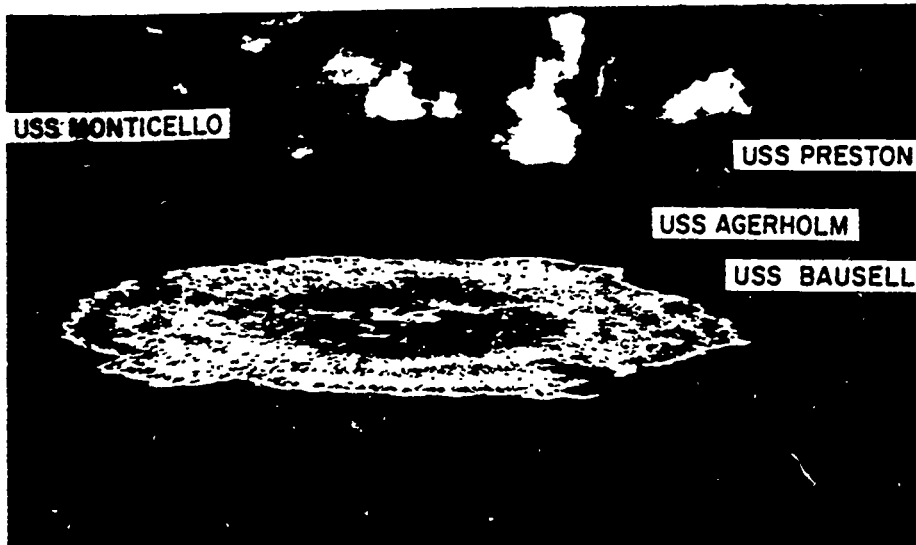at 297 and 329 seconds.

Figure 3.19 Base surge upwind, downwind and crosswind extent.

111

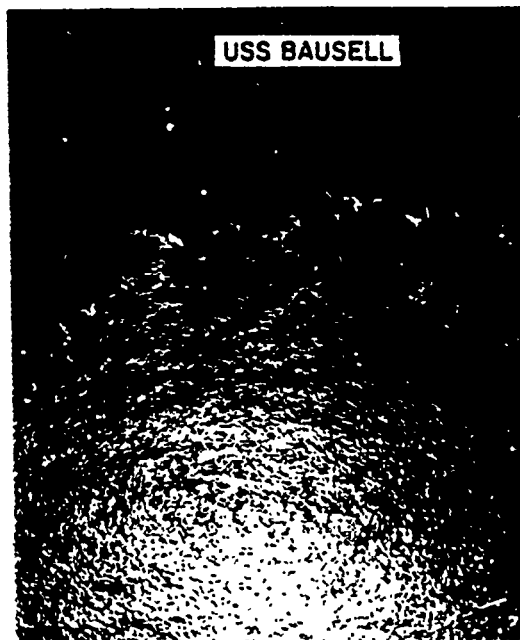6.3 MINUTES

FILM A-2-6

9.7 MINUTES

17.0 MINUTES

FILM A-1B-6

Figure 3.20 Foam patch.

112
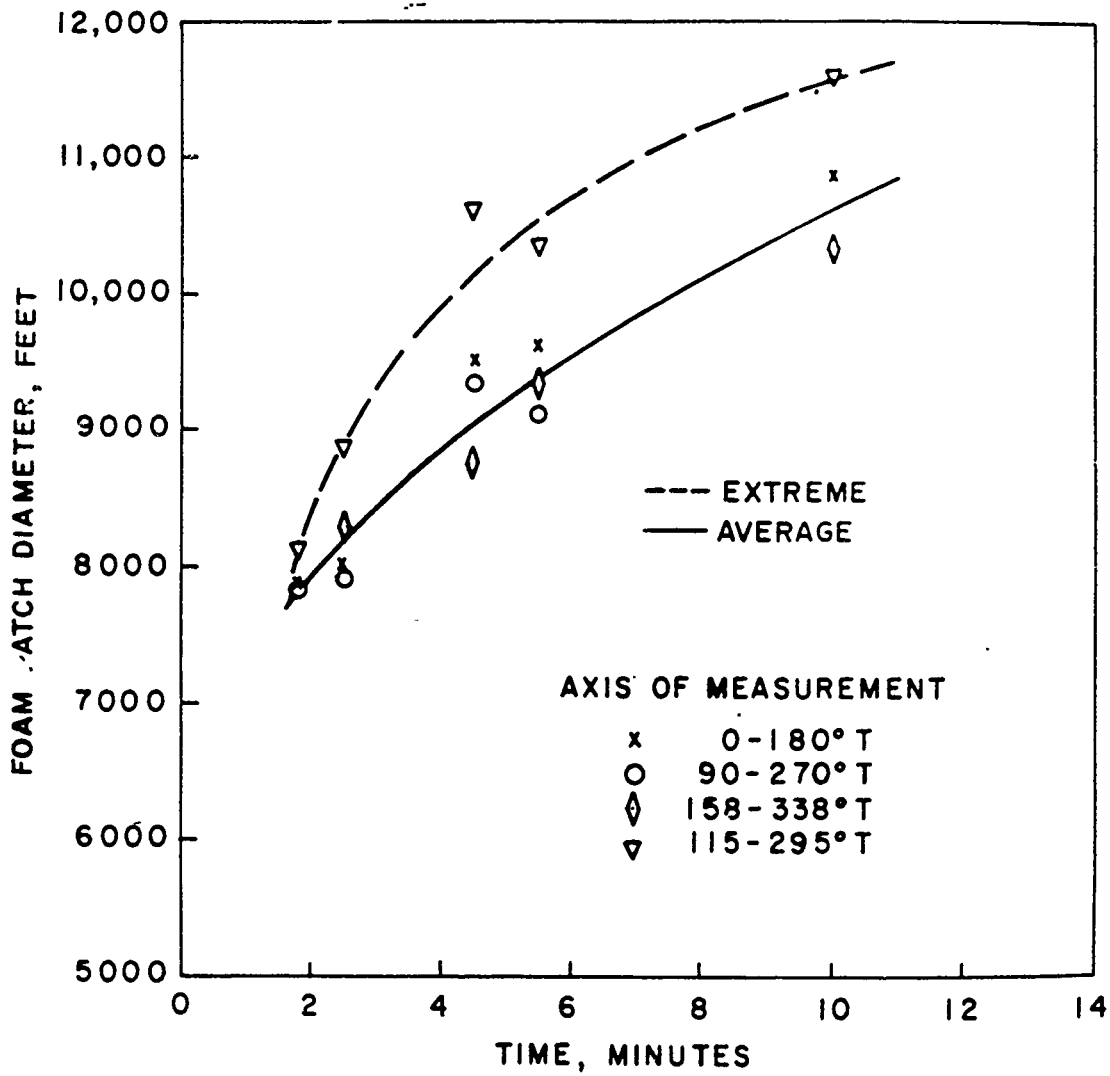
Figure 3.21 Growth of foam patch.

113
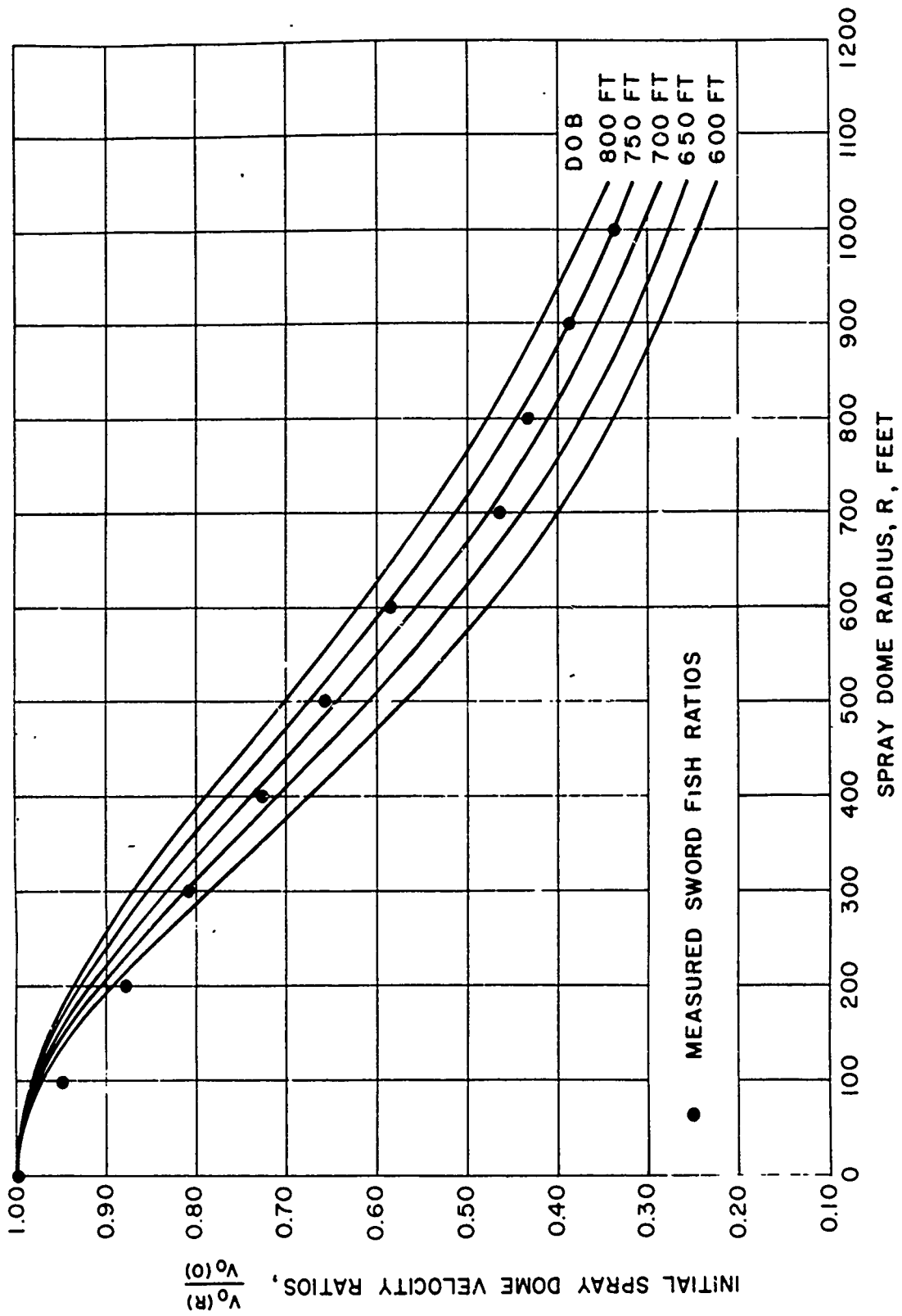
Figure 3.22 Ratios of initial spray-dome velocities for various depths of burst.

114

CHAPTER 4

COMPARISON OF SWORD FISH RESULTS WITH CURRENT PREDICTIONS

4.1 SWORD FISH YIELD AND DEPTH OF BURST

The yield and depth of burst of Sword Fish should be
established before the results presented in Chapter 3 are
compared with existing prediction methods. However, the
precise determination of the experimental conditions may not
be possible. At the time of submission of this report,
Project 1.1 had not determined its final values of yield and
depth of burst. The preliminary values, published in References
1 and 12, were   and 670 ($\pm$30) feet. The radiochemical
yield, determined by Project 2.1, was   (Reference 11). A
depth of burst of 680 feet was determined by Project 1.2,   and
a yield estimate consistent with the radiochemical yield was
obtained from the bubble period as determined from plume
trajectories.

A burst depth of 680 feet wi be used for comparison
purposes and, where possible, comparisons will be made using
both yields. Where this is unwieldy, only the radiochemical
yield will be used.

4.2 SOURCES OF CURRENT PREDICTION METHODS

The prediction techniques currently used have been
briefly discussed in Chapter 1 and are discussed fully in

117

References 4 and 5. As the Sword Fish burst occurred in the deep-burst category (see Section 1.3.2), the dimensions of Shot Wahoo of Operation Hardtack were used as the prototype dimensions for scaling many of the surface phenomena. The prediction methods employed were developed primarily for application to safe delivery tactics and were based on the extreme measurements of Shot Wahoo. The extreme measurements of Sword Fish were therefore used in the comparison.

Bubble migration and period estimates are based on methods given in Reference 10, which result from measurements made on Operation Wigwam and work done with small steam bubbles in a tank.

No attempt will be made to modify the existing prediction techniques, as such changes are beyond the current scope of this type of report. Such improvements, if made, will be reported separately.

4.3 COMPARISON OF RESULTS

Table 4.1 compares the pertinent surface-phenomena measurements observed on Sword Fish with those predicted for yields of   .   at a burst depth of 680 feet. In general, the agreement between the observed and predicted values is within the expected range.

118

4.3.1 Spray Dome. The Sword Fish spray dome, while one of the smoothest observed on a nuclear test, showed the greatest disagreement between observed and predicted dimensions. The initial velocity at surface zero was about

than that predicted for a _____ burst; the retardation factor was _____ and the maximum observed height was _____ that predicted.

The radial extent of the dome, which is a difficult dimension to predict as it is dependent on wave conditions, is within reasonable agreement. The prediction method for this phenomenon is based on the maximum spray-dome radius observed with high explosives. The comparison shown is not strictly valid, since the primary Sword Fish spray dome was produced by the underwater shock wave while the maximum observed extent was increased by the collapse of the cavitated region. Since the spray is only a few feet high in this region, the phenomenon probably is not tactically important.

Reference 4 suggests that, for safety purposes, a 50-percent increase in V_o be used for predictions. Additional safety can be obtained by assuming gravity as the only retarding force. The addition of 50 percent to the predicted initial dome velocity gives a value of _____ and a maximum height of _____ If the retardation due only to gravity is included, the maximum predicted height is

119

The prediction of the size of the spray dome is not
important for ship-delivered weapons such as ASROC; however,
it is an important consideration if such a weapon is delivered
by a low-flying aircraft. A more precise knowledge of the
characteristics of the spray is also needed if spray-dome
measurements are to be used on future tests to estimate yield
and depth of burst.

The lack of adequate prediction methods for the growth
of the nuclear spray dome lies in uncertainties in the theory
and in the methods used to determine values of V_o and f. It
is apparent that Equation 1.4 does not accurately predict the
initial velocity. It is known that surface roughness affects
the initial velocity; exactly how it affects it and if it is
the cause of the anomalous behavior is not known. The problem
of determining values of V_o and f was discussed in Section 3.3.
This problem also must be investigated further before an
adequate prediction technique for delivery tactics and, if
possible, for more precise uses of the spray-dome phenomena,
can be developed.

4.3.2 Primary and Secondary Plumes. A comparison of the
maximum vertical and horizontal extent of the primary plumes
is included in Table 4.1. The observed and predicted height-
vs-time and radius-vs-time curves are compared in Figure 4.1.

120

The maximum observed height was about
than that predicted for a _____ burst. The maximum radial
extent was in almost exact agreement with the predicted extent.
Since Reference 4 gives an accuracy of 30 percent to the
predicted curves, the Sword Fish observed values are well
within the expected range. The times of appearance indicated
in Table 4.1 are in good agreement. These represent the times
at which plume phenomena first became visible in the dome,
therefore the values may differ from the times of origin of
height-vs-time or radius-vs-time curves.

The bubble period and depth of the minimum are in
excellent agreement with those predicted by Reference 10.
Such close agreement was not expected because of the long
plume extrapolations, the fact that the plumes do not
originate at a point, and the photogrammetric problems involved
in determining trajectories from cameras which were in constant
motion.

A prediction method for the maximum height of the secondary
plumes has not been investigated, as such plumes have been
observed only on nuclear tests. The predicted values shown in
Table 4.1 are based on those observed at Wahoo.

4.3.3 Visible Base Surge. A comparison of predicted and
observed crosswind radial extent at various times is included
in Table 4.1. Predictions of the upwind, downwind, and cross-

121

wind base-surge extent are compared with the observed Sword Fish dimensions in Figure 4.2. The predicted upwind extent was obtained by subtracting one-half the wind speed from the crosswind growth curve; the downwind extent was obtained by adding the full wind speed to the crosswind growth. The agreement, in spite of the irregular shape of the surge, is quite good, the greatest difference being less than 10 percent. Reference 4 suggests that a 30-percent safety factor be added to the predicted curves. The Sword Fish values are consistently lower than the predicted curves without this safety factor. Therefore, the current prediction method seems adequate in regard to safety. It may be possible to use the observed Sword Fish curves to extend the current prediction curves, as a longer period of measurement was obtained.

The height of the base surge is difficult to predict, as it depends to a large extent on meteorological conditions. Reference 4 states that a maximum height of from 1000 to 2000 feet should be expected from a deep burst, and the maximum measured Sword Fish height was 1325 feet, although it was probably still increasing when the surge became too diffuse to measure.

4.3.4 Foam Patch. The predicted maximum diameter of the foam patch was 10,000 to 12,000 feet, and was based on the

122

maximum observed diameter of Wahoo. The maximum observed diameter of the Sword Fish foam patch was 11,600 feet at ten minutes after the burst, and it was still expanding at this time. The prediction, while crude, appears to be adequate for this phenomenon.

Page 124-125-126
Deleted

CHAPTER 5

CONCLUSIONS AND RECOMMENDATIONS

5.1 CONCLUSIONS

The success of the project may be evaluated by comparing the results with the objectives presented in Chapter 1. An excellent set of photographic records was obtained, and an adequate number of measurements were made. The only phenomenon not fully documented was the base surge, but Sword Fish was the first nuclear test in which the rectification of the oblique photographs of the base surge was successfully accomplished. Considerable knowledge of this technique was gained for application to other tests of this nature.

The determination of yield, depth of burst, and bubble period from the surface-phenomena measurements was partially successful. However, it revealed areas where current knowledge is not adequate and where accurate measurements must be made in order to obtain reasonable results, particularly in determining the yield. For example, the measured initial spray dome velocity was 12 percent high, yet it produced a yield estimate 31 percent higher than the reported radiochemical yield.

The positions of the ships and platforms in the towed array were determined successfully, although the positions after the burst could not be determined relative to surface zero as its

127

location was not known. In addition, it was possible to estimate, at least crudely, the motion of the tow subsequent to the burst. Information on the flight time, sinking time, and miss distance of the ASROC was also obtained.

The determination of arrival times of the surface phenomena at various stations was partially successful. An insufficient amount of the base-surge data needed to obtain arrival times of this phenomenon at coracles and platforms was obtained. Although not attempted in this report, some correlation between the nuclear radiation recorded at the downwind stations by Project 2.1 and the partial contours presented in this report can probably be found. However, the upwind coracles and platforms were in a pocket of the surge, and it was impossible to determine the base-surge growth within this pocket.

The final objective of this project was to make the Sword Fish results available for improving the existing surface-phenomena scaling and prediction techniques. This objective is met by publication of this report. No attempt to modify the existing techniques has been made, as such efforts are beyond the scope of a FOR.

The need for technical photography, not only for the success of this project but also for the overall success of the operation, was again demonstrated on Sword Fish. Technical photography from the over-head aircraft provided the locations

of the elements in the instrumented array. These locations
were needed by other projects in order to analyze the data
obtained on these elements. Even the ship locations obtained
by shock-wave arrival times, as reported in Reference 1,
depended on the photographically determined locations of the
close-in instrumentation. Pertinent information on the
performance of the missile, including flight time, sinking time,
and miss distance, were also obtained from the overhead cameras.
Information of this nature could not have been obtained
accurately by any other means. Many of the base-surge
measurements needed for scaling purposes were obtained from
the overhead and oblique aerial camera stations. Because of
the irregular shape and cloud-like structure of the surge, this
information cannot be obtained with sufficient accuracy by
cameras located only on ships.

5.2 RECOMMENDATIONS

In spite of the general success of the project, there are
several improvements which should be considered for future
nuclear tests, if conducted. An increased amount of vertical
photography is needed to obtain a complete outline of both the
inner and outer dimensions of the base surge. Because at best
the overhead photography is intermittent, provisions should also
be made to obtain complete contours by means of rectification

of oblique photographs. In this respect, helicopters should be investigated for use as camera platforms. Their ability to hover yields several advantages over a conventional aircraft whose position is constantly changing. The use of helicopters would possibly remove the necessity for radar tracking of these stations.

If other operational-effects tests similar to Sword Fish are conducted, improved methods of operating and aiming the surface cameras should be investigated. One suggestion is presented in Appendix C; another method might be to mount the cameras on gun turrets or platforms. Methods of protecting the photographers eyes from possible retinal burns while viewing the target also require further investigation.

It is possible that the methods used in this report can be employed to rectify oblique photographs obtained on previous underwater nuclear tests, such as Crossroads Baker. It is recommended that these photographs be re-evaluated and, if possible, rectified.

Additional work is needed on some of the prediction methods currently used. The results of Sword Fish probably can be used to extend the base-surge prediction curves for the deep-burst category. Prediction methods for the spray dome also require modification.

A need for additional weapon-effects tests under carefully controlled conditions still exists. If such tests are conducted, they should be adequately funded and have sufficient preparation time. In addition, the firing schedule must be as flexible as possible to insure that the optimum amount of data is obtained.

An important consideration in regard to scheduling is the need for a minimum amount of low cloud cover. On Sword Fish, small cumulus clouds obscured part of the base surge as seen from the air and resulted in a minor loss of data. If the amount of low clouds had been greater, the loss of measurements of the array and of the phenomena could have had serious consequences. A considerable period of delay would be justified in order to avoid such an occurrence.

APPENDIX A

GLOSSARY OF SURFACE-PHENOMENA TERMS

Aerosol Crown. The cauliflower cloud from a very shallow high-explosive underwater burst. See "Smoke Crown".

Air Blast Slick. An expanding white disk on the water surface whose leading edge follows closely behind the intersection of the air shock wave with the water. The whiteness results from the generation of spray by the air shock passage.

Base Surge. A toroidal cloud which forms when the column from a shallow burst or the plumes from a deep burst collapse and break up into spray. The cloud expands radially along the surface of the water, gradually breaking up into separate lobes. On a nuclear burst, part of the radioactive fission debris becomes mixed with the water droplets in the base surge. When the water evaporates, the fission products remain as an invisible cloud or aerosol which continues to expand. The term "base surge" applies to both the visible and invisible clouds. The upwind extent of the surge is measured from surface zero and represents the maximum growth of any lobe in that direction.

132

Base Surge (Cont'd) The crosswind extent is measured perpendicular to the axis of drift, and represents the maximum sideward growth of any lobe. The downwind extent is measured from surface zero and represents the maximum growth of any lobe in that direction. The average radius is the average of all radii measured from the center of the surge. These values are all functions of time. For measurement purposes, a line encompassing all the surge extremities is drawn (see Figure A.1).

Black Ring. See "Dark Ring".

Blow-In. The movement of air into the column if the column walls rupture when the enclosed explosion-bubble contents are below atmospheric pressure. See "Shallow Burst".

Blowout. The escape of explosion-bubble contents to the atmosphere at high pressure, leading to the formation of a cauliflower cloud considerably wider than the column. See "Very Shallow Burst".

Bubble. The globe of gas, vapor, and explosion products which forms when an explosion occurs under water.

133

Carbon Slick. The black patch formed by a very deep high-explosive burst when the carbon rises to the surface.

Cauliflower Cloud. The roughly spherical turbulent cloud which is formed above the column on a very shallow nuclear burst.

Cavitation. The formation of cavities, usually bubbles of air or water vapor, when water is subjected to tensile forces.

Cavitation Pulse Spray Ring. A ring of spray which forms when an underwater pressure pulse, which is generated by the collapse of a submerged cavitated region, reaches the water surface. The ring may be beyond the extent of the primary spray dome.

Central Jet. The narrow vertical plume formed by the convergence of the column walls above a very shallow or shallow high-explosive burst.

Column. A hollow sheath of water thrown upward by the expanding explosion gases formed in a very shallow or shallow burst. The column may be cylindrical or conical in shape.

Column Jets. Plumes which form on an expanding column.

Condensation Cloud. A fog or mist which forms in the rarefaction phase of an air shock wave if adiabatic expansion of the air cools it below the dew-point temperature. Also called a Wilson cloud.

Crack. A rapidly expanding white disk on the water surface whose leading edge follows closely behind the intersection of the underwater shock wave with the surface. The whiteness is believed to be the cavitated region caused by the tension wave which forms and moves downward when the primary shock is reflected from the surface.

Dark Ring. A dark circular region surrounding the spray dome where small isolated jets or spikes of water can be seen if close-up photography is available. The dark appearance is an optical effect caused by the reduced regular reflection of light by the ruffled surface. Under certain conditions of illumination, the ring appears light instead of dark. The ring does not change appreciably in diameter after its formation.

Deep Burst.	An explosion at a depth great enough so that the bubble completes at least one oscillation before it breaks through the surface.
Fallout.	The settling of water drops, particulate matter, or large masses of water ejected into the air by an explosion. Fallout implies a purely vertical motion, except for wind drift, such that falling material deposits directly onto an underlying surface. In a base surge, on the other hand, the motion of drops or particles is predominantly horizontal.
Foam Patch.	A white, roughly circular, area remaining at surface zero after the plumes have collapsed and the surface has ceased to oscillate. The whiteness results from foam and possibly spray at the surface. The patch expands slowly until it disappears.
Foam Ring.	A roughly circular expanding ring of foam remaining at surface zero after the plumes have collapsed and the surface has ceased to oscillate. The ring may constitute the last visible evidence of a foam patch.
Ground Zero.	See "Surface Zero".

Invisible Base Surge. See "Base Surge".

Mound.   The roughly hemispherical upwelling of
                    water appearing after a deep high-explosive
                    test if the bubble arrives at the surface
                    intact, but with no appreciable oscillation.

Near Surface   A nuclear burst which is so shallow that the
Underwater Burst.   water above the explosion is entirely
                    vaporized.

Oblique Plume.   See "Radial Plume".

Plume.   A relatively broad jet or spout of water
                    which disintegrates into spray as it travels
                    through the air. A plume resembles the
                    stream from a fire hose. It always has a
                    dense fluid core. Plumes are generally
                    caused by the pulsation of a bubble in the
                    vicinity of the surface, and appear to erupt
                    from the surface. They also appear on the
                    expanding column formed by a very shallow or
                    shallow burst. More than one phase of plume
                    development may be observed on a single
                    explosion.

Radial Plume.   A plume which emerges from the water surface
                    at any angle except a right angle.

137

Rainout.	The occurrence of rain from a base surge or from the clouds forming above a base surge.
Secondary Plumes.	Plumes which form when the water at surface zero oscillates vertically following the collapse of the primary plumes or column. These plumes form during the rising phase of an oscillation.
Secondary Slicks.	Slicks which form at the water surface with the arrival of a bubble pulse or a bottom-reflected shock wave.
Secondary Spray Domes.	Spray domes which form at the water surface with the arrival of a bubble pulse or a bottom-reflected shock wave.
Secondary Surges.	Base surges which form when the secondary plumes collapse. These surges overtake and merge with the primary base surge.
Shallow Burst.	A burst at a depth which is not sufficient to permit the bubble to complete one oscillation. In this case, the water layer above the explosion, or column, ruptures while the bubble is expanding, but after the bubble pressure has decreased below atmospheric pressure, thus permitting the inflow of air. See "Very Shallow Burst".

138

Slick.

A rapidly expanding ring of darkened water which represents the intersection of the expanding spherical underwater shock front with the surface of the water. In some cases there is an apparent lightening of the water instead of a darkening. The rate of expansion is always in excess of the shock velocity in water.

Smoke Crown.

The cauliflower cloud from a very shallow high-explosive underwater burst. This terminology is used if black smoke is visible in the crown. See "Aerosol Crown".

Spillout.

The spilling over of plumes of water, possibly mixed with bottom material, which occurs around the lip of the cavity formed in the water by a very shallow or shallow burst. These originate from the collapse of the lip.

Splash.

A general term sometimes employed for the surface phenomena of underwater explosions. This has not achieved common usage.

Spray Dome.

A white mound of spray which forms above an underwater explosion when the surface layer rises upward and breaks up into jets, which

Spray Dome (Cont'd)	subsequently disintegrate into water droplets. The spray dome is caused by the reflection of the underwater shock wave. It probably contains a relatively small amount of liquid water.
Stem.	See "Column".
Surface Burst.	An explosion precisely at the surface.
Surface Zero (SZ).	The point on the surface of the land or water vertically above or below the center of an explosion; also called ground zero (GZ).
Surface Zero Time (SZT).	The time at which visible explosion effects appear at the water surface (not including underwater luminosity).
Throwout.	The ejection of debris, weapon fragments, stones, and other missiles by an explosion.
Total Containment Depth.	The depth of burst from which the explosion products do not rise to the surface in any form.
Venting.	The emergence or release of explosion products to the air by any means (blowout, subsequent to blow-in, mixed in plumes, etc.)
Vertical Plume.	A plume which rises vertically from the water surface.

| Very Deep Burst.	An explosion at a great enough depth so that the bubble breaks up, becomes a vortex ring, or loses its identity before reaching the surface.
Very Shallow Burst.	A burst which is shallow enough to permit the explosion bubble contents to emerge at high pressure when the water layer above the burst ruptures. See "Blowout".
Wilson Cloud.	See "Condensation Cloud".
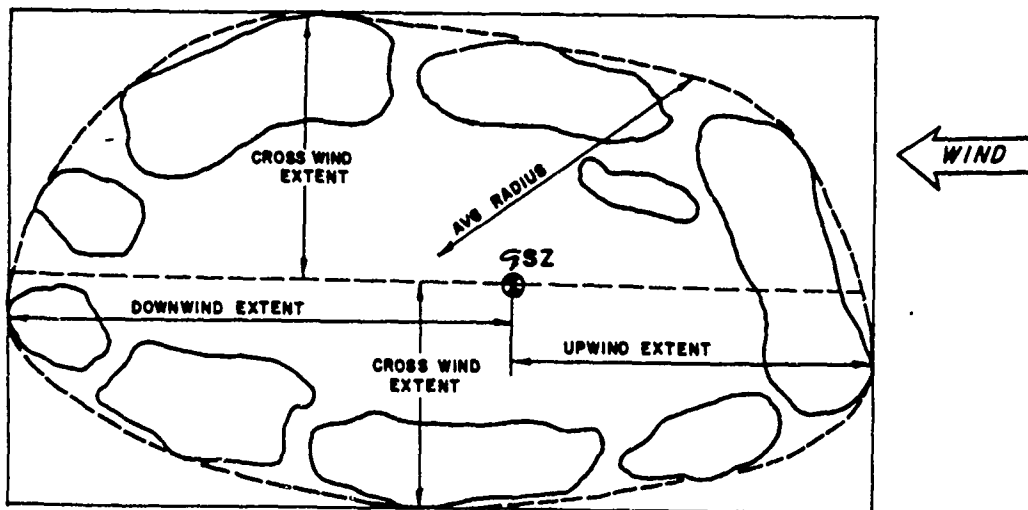
Figure A.1 Base surge (late stage after toroid has broken up).

APPENDIX B

ENVIRONMENTAL DATA

Meteorological Data at 1300 PDT (Recorded on USS Monticello)

Cloud Coverage (total sky)	0.6
Cloud Coverage (above surface zero)	0.2
Cloud Height	2000 feet
Visibility	15 miles
Barometric Pressure	30.3 in. Hg
Air Temperature	60.5 degrees F
Wet Bulb Temperature	52.5 degrees F
Relative Humidity	58 percent
Surface Wind Direction (smoke plume on target)	310 degrees True
Surface Wind Speed (USS Agerholm)	10.5 knots
Surface Wind Speed (smoke plume on target)	10 knots

Upper Wind Observations at 1100 PDT

Height	Wind Direction	Wind Velocity
feet	degrees True	knots
1000	350	07
2000	320	08
3000	310	10
4000	290	10
5000	270	09

Oceanographic Data

Waves	3 feet high, crest to trough, from NW
Swells	1 to 6 feet high, from NW
Surface Current	0.5 knot from 338 degrees True
Surface Sonic Velocity	4960 ft/sec
Depth of Water	2190 ± 10 fathoms
Water Temperature	63 degrees F
Salinity	33.54 parts/thousand

Radiosonde Data at 1700 PDT

Height	Pressure	Temperature	Relative Humidity
feet	millibars	degrees F	percent
Surface	1020	60.4	68
570	1000	57.6	67
3200	908	44.2	64
4770	850	37.2	76

142

APPENDIX C

AUTOMATING THE CAMERAS USED ABOARD SHIP

by

Valmore F. DeVost, U. S. Naval Ordnance Laboratory

The accuracy of field test data obtained photographically depends to a large extent on the precision with which cameras can be trained on the target. Project 1.2 manually trained all its cameras. Generally, if it is possible to get experienced personnel to operate the cameras, this method is reasonably satisfactory. However, when cameras must be operated from the moving deck of a ship and the possibility of an accidental air burst exists, it would be desirable to control the cameras automatically.

It is suggested that on future tests, where combat ships are used as a base of operations, ships' gun fire control systems be utilized as camera platforms wherever feasible. On Sword Fish, for example, all destroyers were equipped with Mark 37 Gun Fire Control Systems. The system's radar may be utilized to support two or three large cameras, similar to the 35mm Mitchells used by Project 1.2, plus several smaller cameras. The system is equipped with power to handle most camera requirements and has intercommunication facilities.

143

The technique of using gun fire control radar aboard Naval ships to train cameras is not new. It is frequently used by the fleet in photo triangulation for anti-aircraft gunnery exercises (Reference 16). In this application one camera is mounted on the ship's radar and locked on target during the exercise. The Naval Ordnance Test Station at Inyokern, California, uses a similar technique for their Radar Boresight Camera Facility (Reference 17). On Sword Fish, a closed-circuit TV camera was mounted directly to the Mk 37 radar reflector to monitor the test from a safe location below decks. The system gave near-perfect stabilization for even the close-up (telescopic lens) coverage.

Figure C.1 illustrates the general layout of the Mk 37 Fire Control Radar Turret and the proposed location of cameras. The radar antenna provides the best mount for three-axis stability. However, since the ships on most operations lay broadside to the target, two-axis stability should provide adequate coverage. The One-Man Control and the Range Finder provide two-axis stability. It may be possible to mount cameras in place of the pointers and trainers telescopes. Estimates of the allowable loads for each of the stations are as follows: (1) Pointers and trainers telescopes, 30 pounds; (2) One-man control, 30 pounds; (3) Radar antenna, 100 pounds; and (4) Range finder, 200 pounds.

If it is necessary to support heav'er loads from the antenna to maintain three-axis stability, the camera platform may be designed to rest on the turret. Controlling the platform attitude to coincide with the radar may be accomplished by coupling the platform to the radar control linkage.

Cameras must be installed at a safe distance from the radar reflector to avoid film radiation, or the cameras must be shielded. Cameras installed on the Range Finders must be secured with wide clamp bands to prevent damage to the insulation which covers the device.

Monitoring the position of cameras on a fire control system with closed-circuit TV would make it possible to continuously check the system and give added assurance that cameras were properly trained. Despite the shortcomings of TV photography for such tests, taped TV coverage would provide adequate back-up should conventional photography fail. The system may also have some value in providing quick-look information.
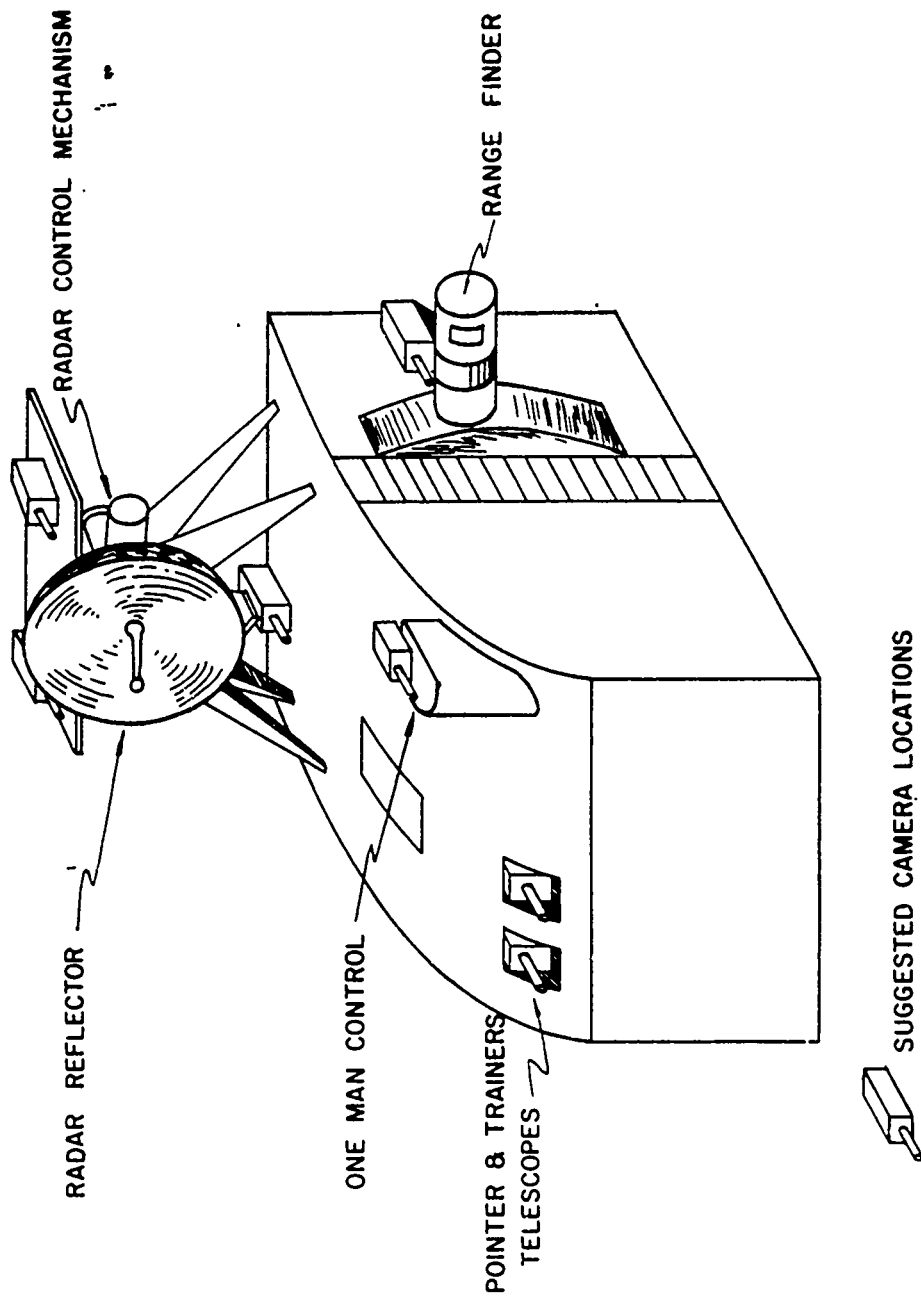
RADAR CONTROL MECHANISM

RANGE FINDER

RADAR REFLECTOR

ONE MAN CONTROL

POINTER & TRAINERS TELESCOPES

SUGGESTED CAMERA LOCATIONS

Figure C.1 MK 37 fire control radar turret.

146

REFERENCES

1. W. W. Murray; "Scientific Director's Summary Report (U)";
Operation Dominic, Shot Sword Fish, POR-2007, 21 January 1963;
David W. Taylor Model Basin, Washington 7, D. C.; Secret
Restricted Data.

2. "Report of The Technical Director, Operation Crossroads";
1947; Volumes I and II; Secret Restricted Data.

3. G. A. Young, J. F. Goertner, and R. L. Willey;
"Photographic Measurements of Surface Phenomena"; Project 1.5,
Operation Wigwam, WT-1009, October 1956; U. S. Naval Ordnance
Laboratory, White Oak, Maryland; Confidential.

4. E. Swift, Jr., and others; "Surface Phenomena from
Underwater Bursts (U)"; Project 1.3, Operation Hardtack, WT-1608,
March 1962; U.S. Naval Ordnance Laboratory, White Oak, Maryland;
Confidential Formerly Restricted Data.

5. G. A. Young; "Surface Phenomena of Underwater Nuclear
Explosions"; NOLTR 63-111;   U. S. Naval Ordnance
Laboratory, White Oak, Maryland; Secret Restricted Data.

6. H. G. Snay and J. F. Butler; "Shock Wave Parameters
for Nuclear Explosions Under Water"; NAVORD Report 4500, May 1957;
U. S. Naval Ordnance Laboratory, White Oak, Maryland; Confidential
Formerly Restricted Data.

7. R. H. Cole; "Underwater Explosions"; 1948; Princeton University Press, Princeton, New Jersey; Unclassified.

8. A. H. Keil; "Introduction to Underwater Explosion Research"; UERD Report 19-56, December 1956; Underwater Explosions Research Division, Norfolk Naval Shipyard, Portsmouth, Virginia; Confidential. -

9. H. Kolsky and others; "Splashes from Underwater Explosions. Part I - Shallow Charges"; Report UNDEX-118, 1 December 1944; Imperial Chemical Industries, Limited, Great Britain; Confidential.

10. H. G. Snay; "The Hydrodynamic Background of the Radiological Effects of Underwater Nuclear Explosions"; NAVWEPS Report 7323, 29 September 1960; U. S. Naval Ordnance Laboratory, White Oak, Maryland; Confidential.

11. L. E. Egeberg, L. D. Johnson, and N. H. Farlow; "Radiological Effects from an Underwater Nuclear Explosion"; Project 2.1, Operation Dominic, Shot Sword Fish, POR 2004, 14 June 1963; U. S. Naval Radiological Defense Laboratory, San Francisco 24, California; Secret Restricted Data.

12. "Underwater Pressures (U)"; Operation Dominic, Shot Sword Fish, Project 1.1, POR-2000; U.S. Naval Ordnance Laboratory, White Oak, Silver Spring, Maryland; Secret Formerly Restricted Data.

13. "Manual of Photogrammetry"; Second Edition, 1952, pages 337-342; American Society of Photogrammetry, Washington, D. C.; Unclassified.

14. D. E. Phillips; "Rectification of Oblique Photographs to Obtain Base Surge Contours"; To be Published as an NOLTR; U. S. Naval Ordnance Laboratory, White Oak, Maryland; Confidential.

15. A. H. Bowker and G. J. Liberman; "Engineering Statistics"; 1959; Prentice-Hall, Inc., Englewood Cliffs, New Jersey; Unclassified.

16. "Photographers Mate I and C Training Manual"; NAVPERS 10375, Chapter 13; Bureau of Naval Personnel, Department of the Navy, Washington, D.C.; Unclassified.

17. J. R. Tracey; "NOTS Assessment Facilities"; NOTS 911; NAVORD Report 3348; 4 August 1954; U. S. Naval Ordnance Test Station, China Lake, California; Unclassified.

pages 151 + 152 deleted